IMPROVEMENT OF TREATMENT FOR PROSTATE CANCER AND PLK1'S ROLE IN NON-SMALL-CELL LUNG CARCINOMA

by

Yifan Kong

A Thesis

Submitted to the Faculty of Purdue University

In Partial Fulfillment of the Requirements for the degree of

Doctor of Philosophy
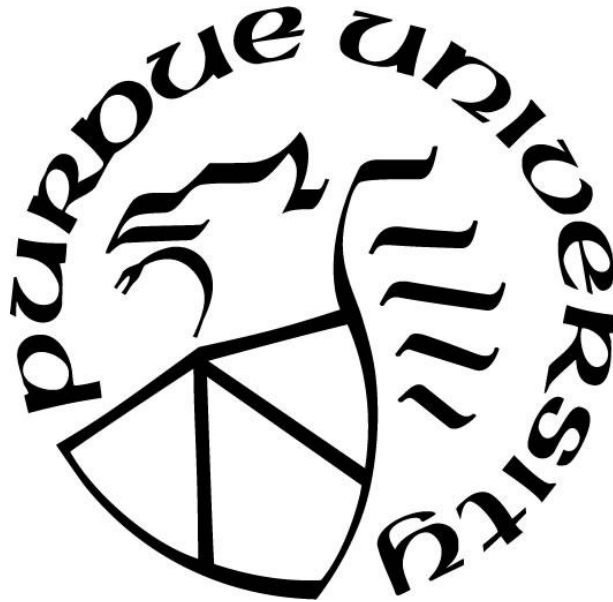
Department of Animal Sciences

West Lafayette, Indiana

May 2020

THE PURDUE UNIVERSITY GRADUATE SCHOOL
STATEMENT OF COMMITTEE APPROVAL

Dr. Shihuan Kuang, Chair

College of Agriculture

Dr. Xiaoqi Liu

College of Medicine (Univeristy of Kentucky)

Dr. Ourania M Andrisani

College of Veterinary Medicine

Dr. Ryan A Cabot

College of Agriculture

Approved by:

Dr. Zoltan Machaty

Dedicated to my parents

ACKNOWLEDGMENTS

First of all, I am deeply grateful to my advisor Dr. Xiaoqi Liu, for without his education, guidance, trust, patience and support, none of these would have happened. He always guided me to be professional and do the right thing.

I also want to express my sincere thanks to Dr. Shihuan Kuang, for all help and suggestions he gave me. Without his guidance, the road would have been tough.

I would like to acknowledge my committee members - Dr. Ourania M Andrisani and Dr. Ryan A Cabot, both of whom has provided patient advice and guidance throughout the whole process of my study and research.

Finally, I thank all my labmates, who have been journeyed with me in these years, for all help and support from them.

TABLE OF CONTENTS

LIST OF FIGURES

LIST OF ABBREVIATIONS

The abbreviations used are:

CRPC: castration-resistant prostate cancer

HMGCR: 3-hydroxy-3-methyl-glutaryl-CoA reductase

AR: androgen receptor

PCa: prostate cancer

ADT: androgen deprivation therapy

HMGCR: 3-hydroxy-3-methyl-glutaryl-coenzyme

EZH2: enhancer of zeste homolog 2

PRC2: Poly Repressive Complex 2

H3K27me3: histone-3 lysine 27 trimethylation

NSCLC: non-small-cell lung cancer

FDA: the U.S. Food and Drug Administration

LADC: lung adenocarcinoma

RET: rearranged during transfection

PLK1: polo-like kinase

MAPK: mitogen-activated protein kinase

CI: combination index

miR: microRNA

MRI: magnetic resonance imaging

ABSTRACT

Prostate cancer (PCa) is the second leading cause of cancer related deaths in American men. In this study, I identify two combinational therapeutics to treat PCa – the combination of enzalutamide and simvastatin, and the combination of GSK126 and metformin, both of which strongly suppress PCa cell growth in vitro and in vivo via inhibiting androgen receptor (AR), an important oncogenic driver for the PCa progression. Simvastatin leads to more AR degradation when combined with enzalutamide. For the combination of GSK126 and metformin, the interaction between enhance of zeste homolog2 (EZH2) and AR is interrupted by GSK126, re-sensitizing EZH2 to metformin. Meanwhile, GSK126 inhibits EZH2's activity.

Polo-like kinase 1 (PLK1), a cell cycle regulator, is usually overexpressed in non-small-cell lung cancer (NSCLC). Here, we report that PLK1 overexpression promotes the development of $Kras^{G12D}$ and $Trp53^{fl/fl}$ (KP)-driven lung adenocarcinoma (LADC). KP mice harboring transgenic PLK1 (KPPI) display heavier tumor burden, poorer tumor differentiation, and lower survival than KP mice. Mechanistically, PLK1 overexpression enhances the activity of MAPK pathway, via upregulating RET expression in a kinase-dependent manner. Supporting our findings, PLK1 knockout in KP mice reduces RET gene expression, inhibits MAPK pathway activity, and strongly delays LADC development. Therefore, these data reveal that PLK1 functions as an oncogene in KP-driven LADC.

CHAPTER 1.   INTRODUCTION

1.1   Prostate cancer (PCa)

PCa is the second leading cause of cancer related death in American men (1). The incidence of it is closely correlated with age, and most patients are diagnosed beyond the age of fifty (2). Androgen deprivation therapy (ADT) becomes the first-line treatment for metastatic PCa, due to the important role androgens play in PCa progression (3). ADT exerts its function either through suppressing androgen synthesis or through inhibiting AR's activity. For example, LHRH agonists and antagonists are used to inhibit PCa progression by downregulating testosterone production in testicles, while another class of drugs, including bicalutamide, flutamide and enzalutamide, inhibits PCa progression by preventing androgen binding to AR (2). Although patients usually benefit from the effectiveness of ADT at the beginning of the treatment, acquired drug resistance usually occurs. When the disease continues to progress despite ADT, the condition is referred to as castration resistant prostate cancer (CRPC) (2, 4).

1.2   Androgen receptor

Androgen receptor (AR) is a ligand-dependent transcription factor, and composed of three domains: a ligand binding domain, a DNA binding domain and an N-terminal domain (2). It is activated after binding to androgen. Activated AR translocates into the nucleus, recruits co-activators and then binds to androgen response elements (ARE), inducing transcription of androgen-regulated genes which play important roles in PCa progression, such as PSA, TMPRSS2, CDK1, CDK2, FGF8 and PMEPA1 (2). Treatments for PCa usually targets androgen biosynthesis or activity of AR. However, Reactivation of AR, including AR overexpression, site mutation, and AR splice variants, can confer PCa cells resistance to the treatments (5-7).

1.3   AR signaling in PCa

Abnormal AR signaling plays a vital role in PCa development. It has been shown that AR is necessary for tumor cell growth, survival and metastasis in both benign and advanced PCa (8). There is a balance between proliferation and apoptosis in normal prostate cells, but it is broken in

PCa tumor cells (9). The mechanism underlying transformation of AR signaling in PCa still remains obscure. Gene fusions of AR targeted genes often happens in PCa tumor cells. For instance, the androgen response elements of TMPRSS2 can fuse to the coding sequence of proteins from Ets family (10), which results in high expression of Ets members driven by AR.

Given that PCa is a disease characterized by activation of AR signaling pathway, it is urgent to develop novel therapeutic methods targeting AR signaling. Despite patients benefit from these treatments initially, acquired drug resistance usually occurs, which is intractable. four major mechanisms underlying the drug resistance often occur (11, 12): (1) De-differentiation to neuroendocrine tumors; (2) AR independent activation of AR downstream signaling pathways, for instance glucocorticoid receptor can take place of AR to regulate its downstream signaling; (3) AR reactivation, including AR site mutations, AR amplification and AR splice variants; and (4) the aberrant metabolism, such as enhancement of endocrine androgens and increasing glycolysis. There might be potential involvement of activation of PI3K signaling in the mechanisms mentioned above.

1.4   HMGCR and cholesterol

3-hydroxy-3-methyl-glutaryl-coenzyme A reductase (HMGCR) is the rate-limiting enzyme of the mevalonate pathway, which produces cholesterol and other isoprenoids (13). Cancer cells require cholesterol for their rapid growth and survival due to its following roles: 1) cholesterol is one of the most important components of most cellular membranes; 2) cholesterol is also a component of lipid rafts, which regulate a variety of signaling pathways (14); 3) cholesterol is the precursor of hormones, including androgens, which can drive progression of PCa (15).

Inhibition of HMGCR is the most promising way to block the mevalonate pathway (13). The inhibitors targeting HMGCR are collectively called statins. Statins have been safely used for decades to treat patients with hyper-cholesterolaemia, and they may have anti-tumor function (16).

1.5   PI3K signaling in PCa

Aberrant activation of PI3K signaling pathway has been identified in 42% patients with benign or localized tumors, and in 100% patients with advanced or metastatic tumors (17). The higher PI3K activation is usually closely correlated with PCa progression, drug resistance and poor patient survival rate (18). It has been demonstrated that PCa could be initiated by PTEN loss of function, which results in high activation of PI3K pathway. Several mouse models to study PCa are designed based on this mechanism, and the mice carrying either heterozygous or homozygous mutations of PTEN can be used to cross with other mice with interest genes to investigate their functions in PCa progression (19). In addition, it has been shown that the PI3K pathway can be activated mainly through the p110β isoform of the PI3K subunit in PCa (20). Blocking p110β, instead of p110α, can downregulate the downstream signaling of PI3K pathway. However, p110β inhibition alone can only be effective for a short time, and fail with emergence of re-activation of PI3K pathway. This is because inhibiting p110β induces feedback upregulation of downstream signaling via p110α (21). Furthermore, compared with inhibiting p110β alone, the combination of inhibitions on both p110α and p110β can induce more persistent inhibition on PI3k signaling, as well as stronger inhibition on tumor growth.

The activation of PI3K signaling pathway is closely associated with the progression of CRPC, indicating that there might be potential interaction between PI3K signaling and AR signaling. In addition, the activation of PI3K determines tumor cells' response to AR antagonists in PCa cancer with PTEN mutation.

1.6   Metformin

Metformin (N, N-dimethylbiguianide), with limited side effects and good safety profile, has been used to treat type II diabetes for decades. Recently, accumulating observational and cohort studies have indicated that diabetes patients treated with metformin exhibited lower incidence of cancer (22), suggesting metformin might be repurposed as an anti-cancer drug. For PCa, a growing amount of evidence shows that metformin decreased PCa incidence and slowed down CRPC progression (23, 24). In a phase II trial, it was observed that PSA secretion was reduced upon

metformin in metastatic CRPC (25). Moreover, encouraging results from a population-based cohort study found that treatment of metformin after diagnosis of PCa increased patients' survival (26). Taken together, metformin is likely to be a useful medication for PCa, but more research is still needed to further confirm the notion.

1.7 EZH2

Enhancer of zeste homolog 2 (EZH2), the functional enzymatic subunit of the Polycomb Repressive Complex 2 (PRC2), inhibits expression of a variety of genes through catalyzing histone-3 lysine 27 trimethylation (H3K27me3) (27). Recently, a growing number of evidence shows that EZH2 plays a vital role in oncogenesis and tumor progression (28), and blocking EZH2's activity can slow down tumor growth. EZH2 can be targeted for inhibition by GSK126 (GSK2816126), an S-adenosyl-methionine-competitive inhibitor, which has recently been shown effective and well tolerated in lymphoma in a Phase I clinical trial (29). Besides EZH2's conventional function, it also acts independently of its methyltransferase activity. For example, EZH2 was reported to form a complex with RelA and RelB to activate nuclear factor κB, in which methylation is not involved (30). Additionally, EZH2 enhances the expression of AR by binding to its promoter, which also doesn't rely on methylation (31). Therefore, novel therapeutics should be identified to decrease EZH2's protein level, although several EZH2 methyltransferase inhibitors, including GSK126, are proved effective.

1.8 Lung cancer

Lung cancer is the leading cause of cancer-related death in the United States, with 228,150 new cases and 142,670 deaths estimated in 2019 (32). Among all cases, non-small-cell lung cancer (NSCLC) amounts for the vast majority. Until now, various molecular targets or oncogenic driver mutations has been identified, including EGFR, ALK, Kras, p53, RET (33). Although drugs designed as inhibitors targeting these molecules has significantly benefited the patients of NSCLC, acquired or de novo resistance often occurs. Therefore, a better understanding of the molecular mechanisms of the disease is needed to develop more effective therapeutics.

1.9 PLK1

Polo-like kinase 1(PLK1) is a serine/threonine kinase which plays an important role in cell cycle regulation. PLK1 is responsible for mitosis entry (34), spindle assembly (35), kinetochore function (36), centrosome maturation (37), cytokinesis (38), APC/C activity (39), and other additional functions. Given the nature of PLK1 and its involvement in mitotic process, much interest has been raised in basic and clinical study of PLK1. PLK1 is reported to be overexpressed in a wide spectrum of human cancers (40). In NSCLC, PLK1 is expressed at higher levels in NSCLC cell lines or tumors compared to normal human bronchial epithelial cell line or non-tumor tissues, and overexpression of PLK1 is correlated with unfavorable patient outcomes (41, 42). Although small-molecule inhibitors targeting PLK1 have been widely studied in in vitro experiments or clinical trials (43), how PLK1 promotes NSCLC still remains unclear.

1.10 MAPK signaling in NSCLC

MAPKs are members of a family of serine and threonine protein kinases. MAPK plays a critical role in cell proliferation, differentiation and survival (44), by regulating signaling transduction from the cell cytoplasm to the nucleus, which is stimulated by binding of extracellular molecules to their receptors, including cytokines, hormones and growth factors. MAPK have three main subfamilies: (1) Ras/Raf/MEK/ERK, which is regulated by extracellular molecules; (2) JNK (the c-Jun N-terminal kinases); and (3) MAPK14 (45). Among these three subfamilies, Ras/Raf/MEK/ERK plays the most important roles in cell proliferation and differentiation.

MAPK signaling dysregulation is closely correlated with the development of NSCLC. In NSCLC, MAPK plays an important role in cell apoptosis, growth and differentiation (44). It has been reported that aberrant MAPK signaling is a frequent event in the development of a variety of cancers, including NSCLC (46). Recently, increasing evidence has shown that MAPK can be used as a prognostic marker of NSCLC, as the high level of MAPK activation is closely associated with high tumor cell proliferation rate, poor tumor cell differentiation, as well as poor patient outcome. Furthermore, MAPK also determines drug resistance by preventing tumor cells from apoptosis (47).

1.11 RET signaling

RET is a tyrosine kinase receptor, which plays a vital role in neurons' survival and differentiation. It can be activated by glial cell-line derived neurotrophic family ligands (GFL) (48). The activation of RET is initiated by extracellular stimulus: the binding of GFLs to their glycosylphosphatidylinositol (GPI)-anchored co-receptors which belongs to GDNF receptor-α family (GFRα) (49). Then, RET can be recruited to the GFL- GFRα complex, inducing activation of RET's kinase domain, followed by auto-phosphorylation (49). Like other tyrosine receptor kinases, RET can regulate a variety of signaling pathways, mainly including MAPK pathway, PI3K pathway, and JNK-STAT pathway (50). Interestingly, all the three important pathways are activated by the same phosphorylated site-tyrosine 1062 (51, 52). It has been shown that RET regulates tumor cell proliferation, differentiation, and metastasis (53). Aberrant RET signaling, including RET point mutations, RET fusions and RET overexpression, is found involved in the development of various human cancer (thyroid, breast, lung) (49). In lung adenocarcinoma, RET fusions, such as CCDC6-RET, TRIM33-RET and KIF5B-RET were identified in ~2% cases (54, 55).

CHAPTER 2.   MATERIAL AND METHODS

2.1   Cell culture, chemicals and reagents

LNCaP, C4-2, 22Rv1, MR49F, C4-2R, PC3-Neo and PC3-AR were used in this study. LNCaP and 22Rv1 were purchased from ATCC. C4-2 was obtained from M. D. Anderson Cancer Center. MR49F and C4-2R were kindly provided by Dr. Amina Zoubeidi at the Vancouver Prostate Cancer Center and Dr. Allen Gao at University of California at Davis, respectively. PC3-Neo and PC3-AR were kindly provided by Dr. Kerry Burnstein (University of Miami). Mouse lung tumor cell lines were isolated from transgenic mice 12-14 weeks after Ad-Cre infection. All cells were grown in RPMI 1640 medium supplemented with 10% fetal bovine serum (FBS) in a humidified incubator at 37°C with 5% CO_2. C4-2R and MR49F cells were maintained in previously described medium containing 20 and 10 µM enzalutamide, respectively. All cells were within 50 passages and Mycoplasma were detected every 3 months using MycoAlert™ PLUS Mycoplasma Detection Kit (Lonza, LT07-705). Enzalutamide and simvastatin were purchased from Medchem Express. R1881 was purchased from Sigma, metformin and GSK126 were obtained from Selleckchem.

2.2   Antibodies

Antibodies against androgen receptor (5153S), cleaved-PARP (9541L), p-AKT (S473) (4051S), AKT (4691S), p-S6 (S235/236) (2211S), p-S6 (S240/244) (5364S), S6 (2317S), p-4EBP1 (T37/46) (2855S), GAPDH (2118L) and cleaved-caspase 3 (9661S) were purchased from Cell Signaling Technology. Antibody Millipore. Antibody against SREBP-2 (sc-5603) was obtained from Santa Cruz Biotechnology.

2.3   Immunoblotting (IB)

Upon harvest, cells were suspended with TBSN buffer (20 mmol/L Tris-HCl, pH 8.0, 0.5% NP-40, 5 mmol/L EGTA, 1.5 mmol/L EDTA, 0.5 mmol/L sodium vanadate and 150 mmol/L NaCl) with protease inhibitors and phosphatase inhibitors, sonicated and then collected, followed by protein concentration measurement by Protein Assay Dye Reagent from Bio-Rad. Equal amounts of protein lysates from each sample were mixed with SDS loading buffer, resolved by SDS-PAGE,

transferred to PVDF membranes, followed by incubations with appropriate primary and secondary antibodies.

2.4   RNA isolation and quantitative real-time PCR (qRT-PCR)

Total RNA was extracted from tissues or cells using RNeasy® mini kit (Qiagen) and reverse transcribed into cDNA using miScript II RT kit (Qiagen). FastStart Universal SYBR Green Master (Roche) was used to measure the expression level of mRNA. Primers used are EZH2, tccctagtcccgcgcaatgagc (forward), ttgttggcggaagcgtgtaaaatc (reverse); β-actin, agaactggcccttcttggagg (forward), gtttttatgttctatggg (reverse). For the detection of microRNAs, specific primers (MS0029239, MS00008372, MS00031220, MS00003122, MS00003129) were purchased from Qiagen, and cDNA was amplified using miScript® SYBR® Green PCR Master Mix (Qiagen). The relative expression level of miRNA or mRNA was normalized to RNU6-2 or β-actin, respectively.

2.5   Colony formation assay

~500 tumor cells used in this study were seeded in 6-well plates with 2ml RPMI 1640 supplemented with 10% FBS. One day later, the medium was replaced with new medium containing different drugs. After 12 days, the colonies were fixed by 10% formalin and stained with 5% crystal violet. Colony numbers were counted by using Image J software.

2.6   Cell viability assay

2500 – 5000 tumor cells used in this study were seeded into 96-well plates, and treated with different drugs with indicated concentrations for 72 hours, followed by incubation with the tetrazolium dye MTT 3-(4, 5-dimethylthiazol-2-yl)-2, 5-diphenyltetrazolium bromide for 4 hours. After the purple formazan was dissolved by DMSO, absorbance at 570 nm was measured by a plate reader.

2.7 Combination index

Cytotoxicity of the drugs was evaluated via determining viability by MTT assay. Combination indice (CI) were calculated by the multiple drug effect equation of Chou (17). $CI = (D)1/(Dx)1 + (D)2/(Dx)2$, where $(Dx)1$ and $(Dx)2$ in the denominators are the doses for metformin and GSK126 alone that gives x% inhibition, whereas $(D)1$ and $(D)2$ in the numerators are the doses of metformin and GSK126 in combination that also inhibited x%. Antagonism is indicated when $CI > 1$, $CI = 1$ indicates an additive effect and $CI < 1$ means synergy.

2.8 ChIP and Re-ChIP

A ChIP assay was performed by using a commercial kit (Millipore, #17-10085) following the manufacturer's instructions. AR binding sites were predicted by PROMO (18,19), and the PCR generated ~200 bp products from the miR-26a-5p proximal (<2,000 bp) promoter containing sites. Antibodies against AR (#39781) and EZH2 (#39901) were purchased from Active Motif. For Re-ChIP, the immunoprecipitated protein-DNA complexes were eluted with Re-ChIP elution buffer (1× TE, 2% SDS, 15 mM DTT) at 37 °C for 30 minutes, and the elutes were diluted 20-fold with ChIP dilution buffer for further incubation with the secondary antibodies and beads. The primers used are: P1, gttgtgggtccaagtacaaatagttttcc (forward), caatatcacctgcctggcctcaa (reverse); P2, gaatttcagaagtttccgtatcccccac (forward), cttttggggtgggtatttgctaaagat (reverse); P3, aattaaaatgaaaattccagtctcctgcctcc (forward), gatggcttttaaaagcatgaagtgtgga (reverse); P4, gcaatagaatgcagaccgatggg (forward), ctatgggagctttctgtccttggc (reverse).

2.8.1 Luciferase assay

HEK293T or PC3 cells were transfected with the indicated plasmids using lipofectamine 2000 (Invitrogen) according to the manufacturer's instructions. Briefly, 0.1 µg of reporter plasmids containing the sequence of interest, together with 5 ng of an internal control plasmid pRL-TK, were transfected into the cells cultured in a 24-well plate. For the expression of AR, EZH2 (S21D) and EZH2 (S21A), the indicated amounts of plasmids were co-transfected into the cells. Total plasmid DNA was normalized to 0.6 µg per well by using an empty plasmid. Luciferase activity

was assayed after 24 hours of transfection using a Dual Luciferase reporter assay system (Promega). The firefly luciferase activities were corrected by the corresponding Renilla luciferase activities and presented as means ± S.D.

2.9   22Rv1-derived mouse xenograft model

All the animal experiments were approved by the Purdue University Animal Care and Use Committee (protocol 1111000133E001). 22Rv1 cells (2.5×10^5 / mouse) were mixed with Matrigel (Collaborative Biomedical Products), and the mixture was injected subcutaneously into right flanks of castrated nude mice (Harlan Laboratories). After two weeks, the tumor-bearing mice were randomized into control and treatment groups (four mice / group).

In the first week, enzalutamide (25 mg/kg body weight) was gavaged, and simvastatin was intraperitoneally injected every 2 days; from the second week, both drugs were administered every day.

Metformin was dissolved in water and administered to mice via oral gavage (30mg / kg body weight / day). GSK126 in 20% captisol with PH adjusted to 4-4.5 was injected intraperitoneally into mice (50mg / kg body weight / day).

Tumor volumes were calculated from the formula $V = L \times W2/2$ (where V is volume [cubic millimeters], L is length [millimeters], and W is width [millimeters]).

2.10 LuCaP35CR xenograft model

Mice bearing LuCaP35CR tumors were obtained from Dr. Robert Vessella at the University of Washington. Tumors were implanted and amplified in pre-castrated NSG mice. When tumor size was big enough, tumors were harvested and cut into ~25 mm3 pieces, followed by implantation into 16 pre-castrated NSG mice. After tumor size reached ~200 mm3, mice were randomized into four groups, followed by similar treatment and measurement as described above.

Histology and immunohistochemistry. Xenograft tumors were fixed in 10% neutral buffered formalin, paraffin-embedded, sectioned to 5 mm, and stained using conventional hematoxylin and eosin (H&E) staining. Immunofluorescent chemistry staining was accomplished with the M.O.M.TM kit from Vector Laboratories.

2.11 PSA measurement

Blood was collected from mice by retro-orbital bleeding, followed by centrifuge to collect serum. PSA levels were determined using a PSA ELISA kit (Abnova KA0208) as manufacturer instructed.

2.12 Statistical analysis

All numerical data are presented as mean ± SD. The statistical significance of the results was analyzed by using unpaired two-tailed Student's t test. P values of <0.05 indicate statistical significance.

2.13 Mouse models

Rosa26$^{LSLPlk1/+}$ mice have been described previously (56). Plk1$^{fl/fl}$ and Plk1$^{fl/+}$ mice were a kind gift from Dr. Guillermo de Cárcer from Spanish National Cancer Research Centre (CNIO), Madrid, Spain (57). Kras$^{LSLG12D/+}$ p53$^{fl/fl}$ (KP) mice were kindly provided by Dr. Andrea Kasinski from Purdue University, USA. A mixture of male and female mice was utilized in all experiments. For studies using adenovirus, Ad-Cre was purchased from University of Iowa, and instilled into mice via intratracheal delivery at a viral titer of 2.5×10^7 PFU per mouse according to the protocol by DuPage et al (58).

2.14 RNAseq

Total RNA was extracted from whole tumors of mice by using RNeasy Mini kit (#74104, Qiagen) according to the manufacturer's instructions. To be specific, only one tumor was harvested from each mouse, and six mice were selected from either group (KP group: 6 tumors; KPPI group: 6 tumors). Then samples were sent to Novogene Biotechnology Company (CA, USA) for RNA quality assessment, RNAseq library construction, Illumina sequencing and data analysis.

CHAPTER 3. INHIBITION OF CHOLESTEROL BIOSYNTHESIS OVERCOMES ENZALUTAMIDE RESISTANCE IN CASTRATION-RESISTANT PROSTATE CANCER (CRPC)

3.1 Introduction

Prostate cancer (PCa) is the second-leading cause of cancer related death in American men. Because its progression is androgen dependent, androgen deprivation therapy (ADT) is the primary approach for the treatment of PCa. Although patients benefit from ADT at the beginning of treatment, most of them will relapse with castration-resistant prostate cancer (CRPC), which is currently incurable. Enzalutamide is a nonsteroidal second-generation antiandrogen that has recently been approved for the treatment of metastatic CRPC both in the post-docetaxel and chemotherapy-naive settings. It can inhibit androgen binding to the androgen receptor (AR), AR translocation into the nucleus, AR binding to DNA and coactivator recruitment (59). While enzalutamide is efficient initially, acquired drug resistance usually occurs inevitably.

Accumulated experimental research suggests that activation of de novo cholesterogenesis induces PCa cell proliferation and promotes cancer development and progression (60-62). Men with higher cholesterol are usually in greater risk of developing high-grade prostate cancer. Mevalonate pathway is known to synthesize cholesterol, and 3-hydroxy-3-methyl-glutaryl-CoA reductase (HMGCR) is the first rate-limiting enzyme of it. Thus, inhibiting HMGCR is traditionally used to lower serum cholesterol as a means of reducing the risk for cardiovascular disease. Inhibitors targeting HMGCR, known collectively as statins, are generic drugs for the treatment of hypercholesterolemia. In addition to statins' efficacy in treating cardiovascular disease, accumulating evidence suggests that statins also exert an anti-neoplastic effect in many types of cancer, including breast, prostate, ovarian, lymphoma, renal cell carcinoma and colorectal cancer (63). In PCa, both in vitro and in vivo experiments showed that statins could significantly reduce the level of prostate-specific antigen (PSA) (64-66). Furthermore, it was reported that such down-regulated PSA levels might be caused by proteolysis of AR induced by statins (67). All these studies suggest that statins may suppress PCa progression through inhibiting AR.

In our study, HMGCR was found to be overexpressed in enzalutamide-resistant cell lines (MR49F and C4-2R). Furthermore, knocking down HMGCR re-sensitized C4-2R to enzalutamide, and HMGCR overexpression renders C4-2 resistant to it. Next, we identified simvastatin could be used to overcome enzalutamide resistance both in vitro and in vivo. Mechanistically, the combination of simvastatin and enzalutamide exerts a synergistic effect on AR protein turnover, which may be induced by simvastatin's inhibition on PI3K pathway.

3.2   Results

3.2.1   Identification of aberrant HMGCR expression in enzalutamide-resistant protate cancer cell lines

To investigate the molecular mechanism underlying enzalutamide resistance, RNA-seq analysis was conducted with LNCaP and MR49F cells. As shown in Fig. 1A, MR49F displayed higher HMGCR expression than LNCaP. To verify it, western blot was performed with LNCaP and MR49F, as well as C4-2 and C4-2R (another pair of cell lines to study enzalutamide resistance, C4-2R is derived from C4-2). As shown in Fig. 1B-D, MR49F and C4-2R showed higher expression levels of HMGCR than their parental cell lines respectively. In addition, such differences became larger and more significant when cells underwent 4-hour enzalutamide treatment (Fig. C and D). Besides HMGCR, we also examined the protein levels of SREBP2, another important molecule of cholesterol synthesis. Upon enzalutamide treatment, MR49F and C4-2R exhibited higher levels of cleaved SREBP2 (the active status) than their parental cell lines respectively (Fig. 1B). Next, we investigated the levels of cholesterol, the product of mevalonate pathway, using the PCa cell lines mentioned above. As shown in Fig. 1F and 1G, significantly higher cholesterol levels were observed in the enzalutamide-resistant cell lines than their parental cell lines after enzalutamide treatment. Collectively, our data demonstrated that HMGCR expression, as well as the amount of cholesterol, was elevated in enzalutamide-resistant cells. To further validate this finding in clinic, the bioinformatics analysis was performed with 72 patient specimens (described under "Experimental procedures"). Accordingly, we found that cholesterol biosynthesis pathway gene set was enriched in high HMGCR-expressing group, indicating that cholesterol biosynthesis pathway was activated as HMGCR expression was elevated (Fig. 1G).

Furthermore, gene set enrichment analysis (GSEA) of the HMGCR expression profile showed that steroid biosynthesis pathway-related gene set is also positively enriched (Fig. 1H).

3.2.2   The HMGCR expression level affects cellular response to enzalutamide

Having demonstrated enzalutamide-resistant PCa cell lines harbored higher HMGCR expression, we want to know whether the cellular response to enzalutamide could be affected by HMGCR. To investigate this, we knocked down HMGCR in C4-2R using shRNA, and HMGCR protein level was determined by IB (Fig. 2A). Due to the low efficacy of single shRNA, a mixed pool of both shRNAs was used to construct stable HMGCR-KD cell line, followed by growth assay to examine cells' response to enzalutamide. As shown in Fig. 2B, C4-2R cells, after HMGCR being knocked down, displayed decreased viability upon enzalutamide treatment. Furthermore, restoration of HMGCR in HMGCR-KD cells apparently rescued cells from enzalutamide-induced growth inhibition (Fig. 2C and D). Consistently, compared with control cells exhibiting no significant difference in colony numbers after enzalutamide treatment (Fig. 2E), fewer colonies were formed by HMGCR-KD cells (Fig. 2F), and the phenotype was largely reversed upon reintroduction of HMGCR (Fig. 2G). Furthermore, immunoblotting against cleaved PARP was conducted to examine cells' apoptosis. As expected, knockdown of HMGCR promoted C4-2R's apoptosis upon enzalutamide resistance (Fig. 2H). To further confirm HMGCR's role, C4-2 was transiently transfected with HMGCR, followed by a 3-day cell-growth assay under enzalutamide treatment. As indicated, more C4-2 cells with HMGCR overexpression survived than the cells carrying pcDNA3.0 (Fig. 2I). Also, we noticed that MR49F and C4-2R, in which the aberrant expression of HMGCR contributes to enzalutamide resistance, were more sensitive to mevastatin, an inhibitor targeting HMGCR, than their parental cell lines respectively (Fig. 2, J and K), providing a possible new approach to overcome enzalutamide resistance.

3.2.3   Simvastatin treatment overcomes enzalutamide resistance in vitro

Simvastatin, one of the marked statins, was used to identify whether it could restore inhibitory effect of enzalutamide on enzalutamide-resistant PCa cells. Firstly, colony formation assay was

performed with MR49F, C4-2R and 22Rv1. As shown in Fig. 3A, 3B, and 3C, fewer colonies were formed by all three cell lines upon the combination of enzalutamide and simvastatin, implying simvastatin can enhance enzalutamide efficacy. To further verify this, proliferation assay was conducted with MR49F and C4-2R. Simvastatin alone slightly slowed down cell growth, while the combination of the two drugs significantly inhibited cell proliferation (Fig. 2D and E). Meanwhile, representative images were taken with C4-2R cells after 5-day treatments to compare potential morphology change. As shown in Fig. 3F, no apparent difference was observed when cells were treated with enzalutamide, but simvastatin induced shrinkage. C4-2R upon the combinational treatment displayed further reduced cell number, as well as the same morphological modification induced by simvastatin alone (Fig. 3F). Next, apoptosis was examined after indicated treatments. The single treatment of simvastatin resulted in relatively weak apoptosis, but the combination of enzalutamide and simvastatin led to higher levels of apoptosis than either treatment alone (Fig. 3G and H).

3.2.4   Simvastatin treatment overcomes enzalutamide resistance in vivo

Next, a 22Rv1 xenograft model was used to investigate whether statins can overcome enzalutamide resistance in vivo. As shown in Figs. 4A, B, and C, compared with control group, 22Rv1 tumors upon enzalutamide treatment displayed limited change of growth rate or tumor size. Simvastatin alone partially inhibited tumor growth, but the combination of simvastatin and enzalutamide strongly inhibited it (Fig. 4A, B and C). Meanwhile, there was no significant difference in mice body weight among all groups (Fig. 4D), implying that the combination of the two drugs didn't induce severe side effects. Histologically, the cells in control and enzalutamide groups were arranged compactly, but loosely upon simvastatin treatment. In contrast, scattered cell groups were found after tumors being treated with the combination of enzalutamide and simvastatin (Fig. 4E, H&E). Furthermore, immunostaining of Ki67 and cleaved caspase-3 substantiated that the combination of enzalutamide and simvastatin exhibited the strongest inhibitory effect on tumor cell proliferation, and led to the most apoptosis compared with other three groups (Figs. 4F, G, H, and I). Collectively, our in vivo results support the notion that enzalutamide's tumor-killing effect was restored by simvastatin.

3.2.5 Simvastatin induces AR degradation

Enzalutamide resistance has been reported to be induced by AR reactivation (6). Considering AR usually plays a vital role in PCa progression and drug resistance, we tried to investigate whether AR is affected by simvastatin. As shown in Fig. 5A, AR protein level was reduced by simvastatin in a dose-dependent manner in C4-2R. Furthermore, our quantitative real-time PCR result showed that there was no significant difference in mRNA expression of AR upon simvastatin treatment (Fig. 5B), indicating that transcription of AR is not affected by simvastatin. Next, cycloheximide (CHX) was utilized to examine simvastatin's effect on protein turnover of AR. After CHX was added to the cells, simvastatin treatment enhanced AR degradation (Fig. 5C). Thus, it is likely that AR degradation can be induced by simvastatin via the ubiquitin-proteasome system. To confirm this, MG132, a 26S proteasome inhibitor, was used to test whether it can reverse the simvastatin-induced AR degradation. As shown in Fig. 5D, AR protein level was partially rescued by MG132 from the degradation induced by simvastatin.

3.2.6 Enzalutamide and simvastatin decrease AR protein expression synergistically

Having established that simvastatin alone enhanced AR protein degradation, we then asked whether the combination of enzalutamide and simvastatin would synergistically affect AR protein level. To investigate this, C4-2R, 22Rv1, and MR49F were treated with enzalutamide, simvastatin at the indicated concentrations or combinations of the two drugs, and harvested for western blot. As shown in Figs. 6A – C, AR protein levels of all cell lines, as well as AR-Vs of 22Rv1, were further decreased by the combinational treatment than simvastatin treatment aloe. In addition, we aimed to confirm that the apoptosis induced by enzalutamide plus simvastatin is due to degradation of AR. Toward that end, AR was overexpressed in all three cell lines mentioned above, followed by the combinational treatment for 48 hours. As shown in Fig. 6D, less apoptosis was observed in cells overexpressing AR, indicating that overexpression of AR can prevent enzalutamide-resistant cells from apoptosis induced by the combination of the two drugs. Finally, to test whether the effects seen above are specific to HMGCR, we examined AR protein expression after knocking down HMGCR. As shown in Fig. 6E, AR level was significantly reduced after treatment of enzalutamide.

3.2.7 Gene expressions of AR and mTOR are positively correlated with HMGCR

Our previous study showed that positive feedback loops exist among mTOR pathway, AR signaling pathway, and lipid biosynthesis pathway (68). Thus, we wanted to test whether such interaction is still active after anti-hormone therapy or even in enzalutamide-resistant cells. To investigate this, Pearson correlation analysis, using 72 anti-hormone treatment patients' samples, was performed to detect the gene expression interaction between HMGCR and mTOR, AR and mTOR, as well as AR and HMGCR. As shown in Fig. 7A-C, all three genes were positively correlated with each other, indicating they are likely to be overexpressed in enzalutamide-resistant cells. Moreover, the mTOR pathway gene set was enriched in high-HMGCR group (Fig. 7D) or high-AR group (Fig. 7E), implying that the whole mTOR pathway is potentially activated in enzalutamide-resistant cells. To confirm our finding from the above analysis, the lysates of LNCaP, MR49F, C4-2 and C4-2R were used to test the molecular change. As shown in Fig. 7F, MR49F and C4-2R displayed higher expression of cleaved SREBP2, HMGCR, AR and critical proteins of mTOR pathway, compared with their parental cell line respectively. Moreover, knockdown of HMGCR inhibited mTOR pathway (Fig. 7G). Then, we asked whether simvastatin can affect mTOR pathway. To investigate this, C4-2R cells were treated with simvastatin at indicated concentrations. After 48-hour treatment, both p-AKT and p-S6 were decreased (Fig. 7H), suggesting simvastatin is capable to inhibit mTOR pathway. More interestingly, the combination of enzalutamide and BKM120, an AKT inhibitor, could induce obvious degradation of AR (Fig. 7I), which can potentially explain why the combination of enzalutamide and simvastatin reduces AR significantly.

3.3 Discussion

Enzalutamide, which has been recently approved by FDA, can significantly improves the therapeutic effect for late-stage CRPC patients (59, 69, 70). However, drug resistance usually occurs. In our study, HMGCR, a key enzyme of mevalonate pathway, was found to be overexpressed in enzalutamide-resistant cell lines (MR49F and C4-2R). Furthermore, knocking down HMGCR re-sensitized C4-2R to enzalutamide, and HMGCR overexpression made C4-2 resistant to it. Next, we identified simvastatin could be used to overcome enzalutamide resistance both in vitro and in vivo. Mechanistically, the combination of simvastatin and enzalutamide exerted a synergistic effect on AR protein turnover, which may be induced by simvastatin's inhibition on PI3K pathway.

Accumulating evidence shows the aberrant biosynthesis of lipid or cholesterol is associated with lethal PCa (71-74), and the lipid biosynthesis induced by AR reactivation can result in resistance to androgen-deprivation therapies (75). For enzalutamide resistance, intracrine androgen synthesis, which provides ligand for AR, was reported to be one of the reasons (76). Consistently, we identified that expression of HMGCR, the first rate-limiting enzyme of cholesterol synthesis, was elevated in enzalutamide-resistant cell lines, and more cholesterol, which might be used to synthesize androgen, was produced to support survival of cells upon treatment of enzalutamide.

Statins' inhibitory effect on PCa cell proliferation has been investigated by several studies. Sekine et al. reported that simvastatin inhibited PC3's proliferation and induce apoptosis (77). Additionally, Hong et al. showed that the proliferation of LNCaP could be suppressed by lovastatin (78). These are consistent with our finding that simvastatin also slowed down the cell growth rate and led to apoptosis of enzalutamide-resistant cells. Meanwhile, we were trying to investigate whether the inhibition on HMGCR could overcome enzalutamide resistance, and our data exhibited that the combination of simvastatin and enzalutamide exerted strong inhibitory effect on MR49F, C4-2R, and 22Rv1, which is consistent with Syvälä et al (79).

In order to investigate the underlying mechanism, we tested the effect of the combinational treatment on AR. Syvälä et al. revealed that simvastatin slightly decreased AR protein level in LNCaP (79), and Yokomizo et al. found AR was downregulated by mevastatin and simvastatin in

RWPE-1, 22Rv1 and LNCaP cells (67). Consistently, our finding shows that simvastatin resulted in slight AR protein degradation via the proteasome system instead of affecting mRNA transcription. Furthermore, we found that the combination of simvastatin and enzalutamide induced more degradation of AR than simvastatin alone. The strong degradation of AR was also observed in HMGCR-KD cells upon enzalutamide treatment. Considering AR site mutation and AR amplification still play vital roles in drug resistance, the combination of enzalutamide and simvastatin, both of which are FDA-approved, can be considered as treatment for CRPC patients.
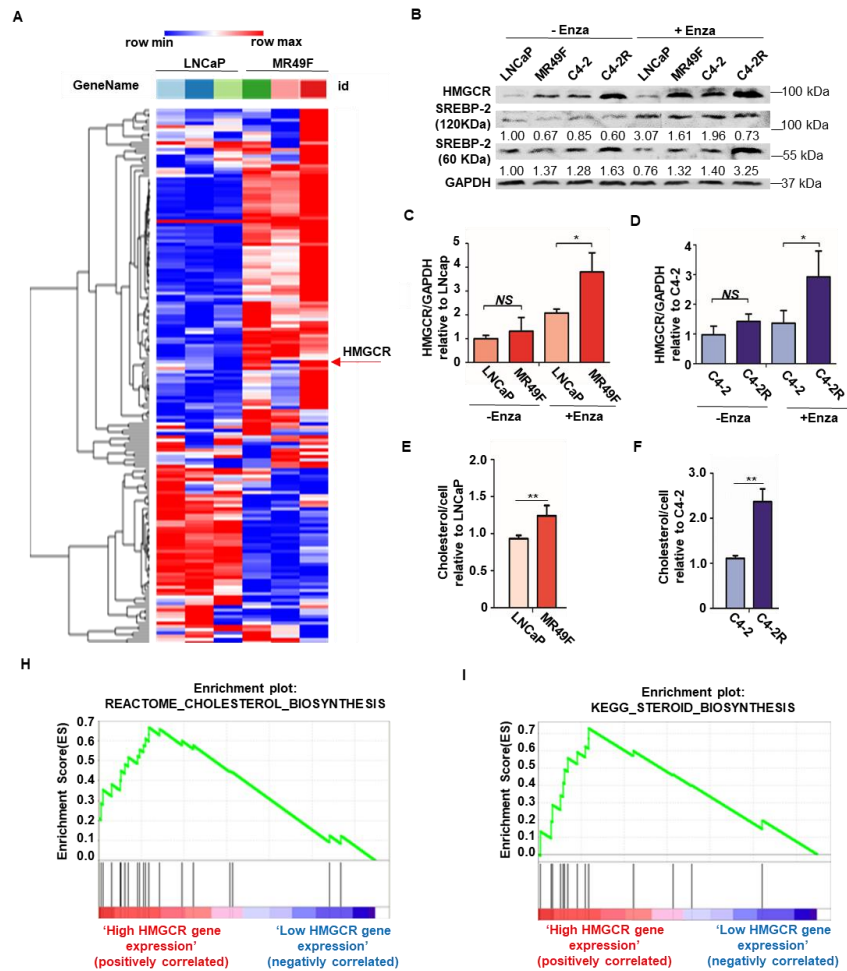
Figure 1. Cholesterol biosynthesis is elevated in enzalutamide-resistant PCa cells

(A) Heat map displaying patterns of gene expression in LNCaP versus MR49F. (B) Indicated PCa cells were treated with DMSO or enzalutamide (10 µM for LNCaP and MR49F; 20 µM for C4-2 and C4-2R) for 4 hours, and then harvested for western blot. (C and D) Quantification of HMGCR in Fig. 1C. Results are represented as mean ± SD, n = 3. (E and F) After cells underwent 4-hour enzalutamide treatment, total cholesterol was extracted and measured by a kit following the manufacturer's instruction. Results are presented as means ± SD. (G) GSEA shows that the gene set of cholesterol biosynthesis pathway is enriched in the high HMGCR-expressing group. (H) GSEA shows that the gene set of steroid biosynthesis pathway is enriched in the high HMGCR-expressing group.
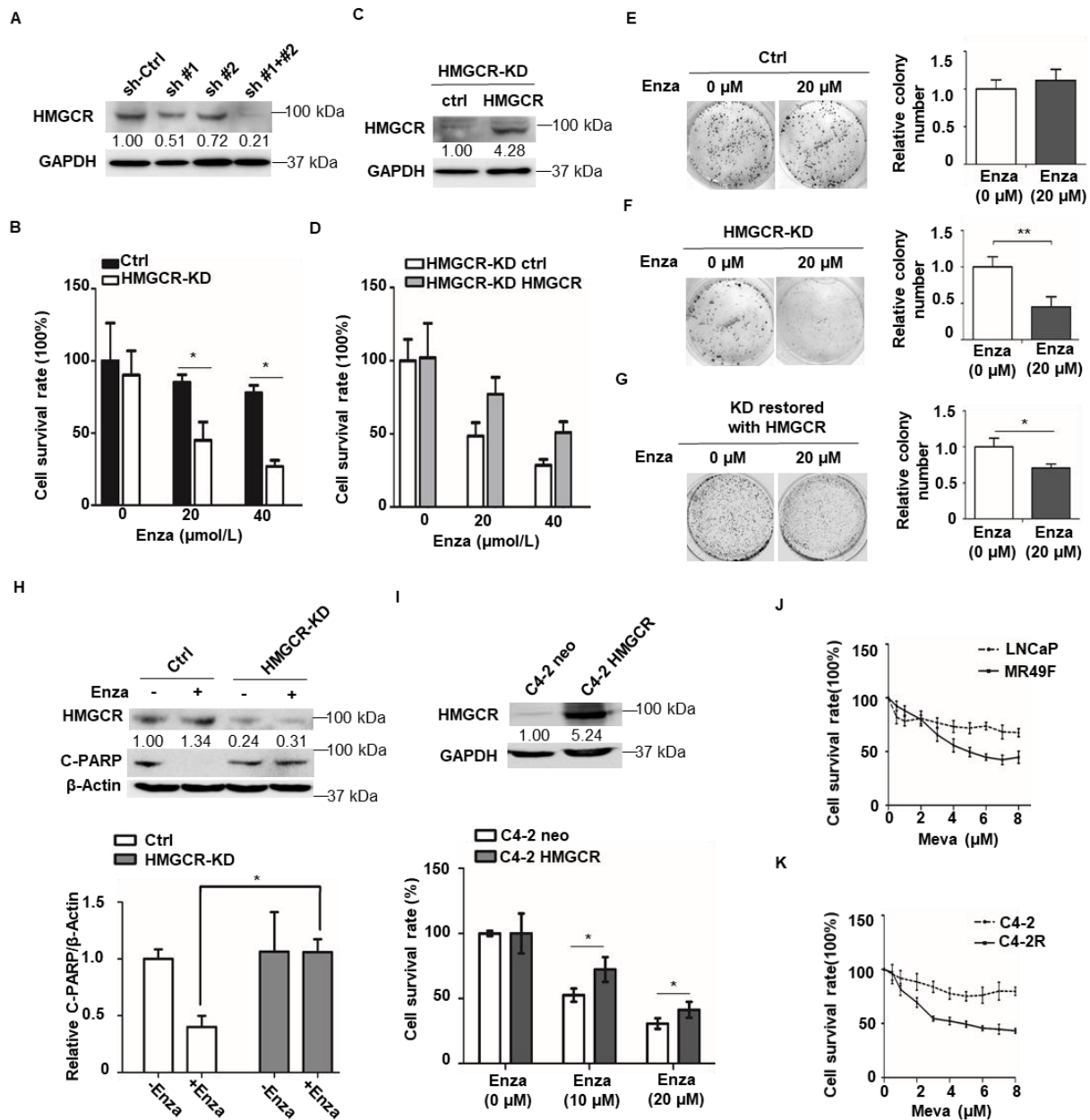
Figure 2. HMGCR confers resistance to enzalutamide in PCa cells

(A) C4-2R was stably transfected with control shRNA or shRNA targeting HMGCR, and harvested for IB. (B) HMGCR-KD C4-2R cells, as well as control cells, were treated with enzalutamide at the indicated concentrations for 72 hours. Then, the cell number was counted. Results are presented as means ± SD. (C) HMGCR-KD C4-2R cells, as well as control cells, were

cultured in the media with DMSO, enzalutamide (20 µM) for 14 days. Then, colonies were fixed using 10% formalin, and stained with crystal violet staining. Results are presented as means ± SD. (D) HMGCR-KD C4-2R cells and control cells were treated with 20-µM enzalutamide or DMSO for 48 hours, and harvested for IB. Bands intensities are quantified and presented as means ± SD. (E) C4-2 cells were transiently transfected with pcDNA3.0 or HMGCR, then treated with enzalutamide at the indicated concentrations for 72 hours, and harvested for cell number determination. Results are presented as means ± SD. Meanwhile, cell lysates were collected for IB to examine the expression of HMGCR. (F and G) The indicated PCa cells were treated mevastatin (Meva) at the indicated concentrations for 72 hours, followed by MTT assay. Results are presented as means ± SD. *, $p < 0.05$.
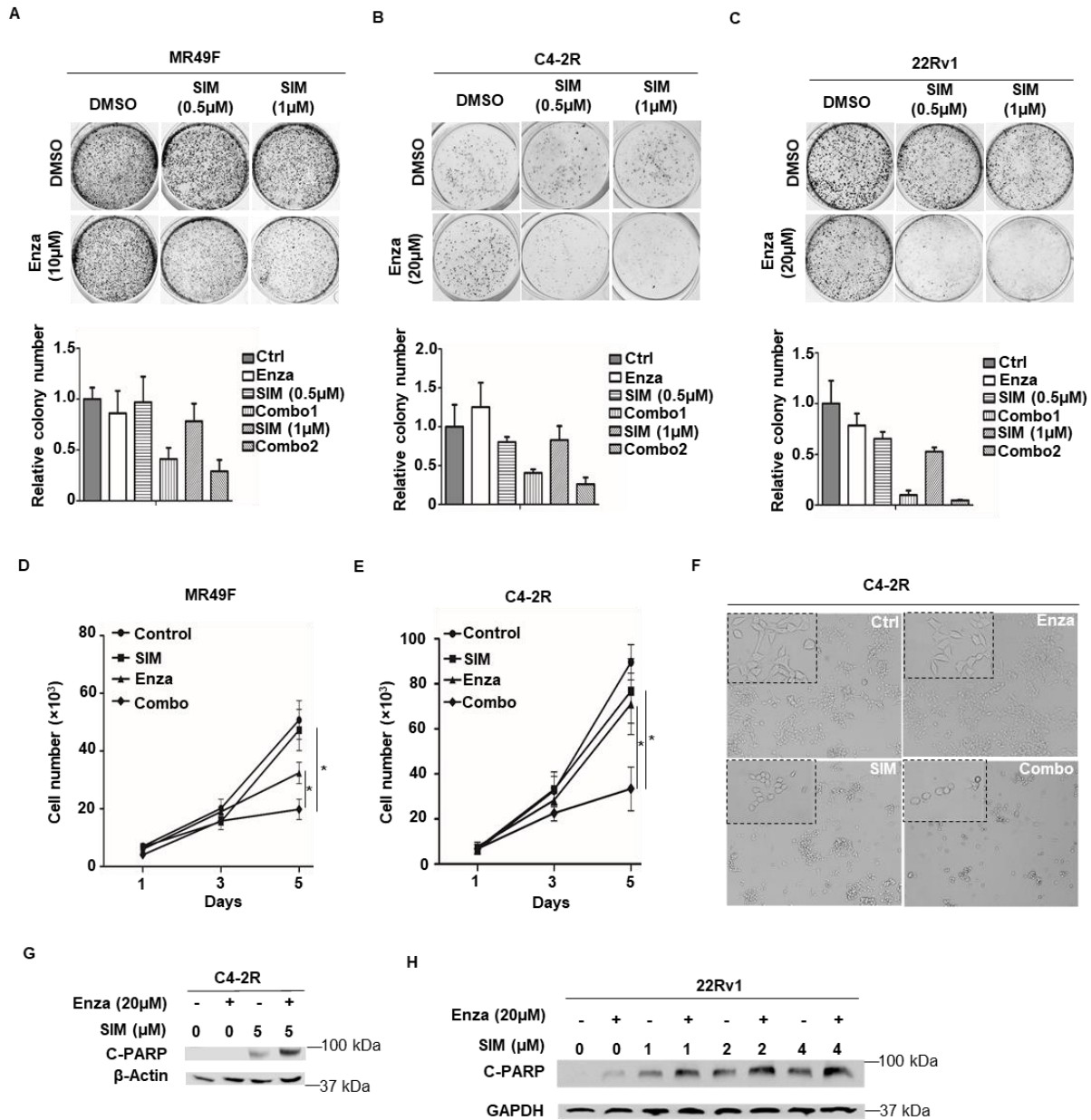
Figure 3. Simvastatin treatment overcomes enzalutamide resistance in vitro

(A-C) MR49F, C4-2R and 22Rv1 (~1000/well) were cultured in the media with enzalutamide, simvastatin, or both drugs at the indicated concentrations. Media was changed every 3 days for 10 days. Then the cells were fixed and stained with crystal violet. Results are presented as means ± SD. (D) MR49F cells (~5000/well) were cultured in the media with enzalutamide (10 μM), simvastatin (1 μM), or both drugs. A 5-day Growth assay was perfomed with cell number being counted every day. (E and F) C4-2R cells (~5000/well) were cultured in the media with

enzalutamide (20 µM), simvastatin (1 µM), or both drugs. A 5-day Growth assay was performed with cell number being counted every day. Representative images were taken on the fifth day to display the morphology of the cells. (G and H) C4-2R or 22Rv1 cells were treated with simvastatin, enzalutamide or both drugs at the indicated concentrations for 48 hours, followed by western blot.
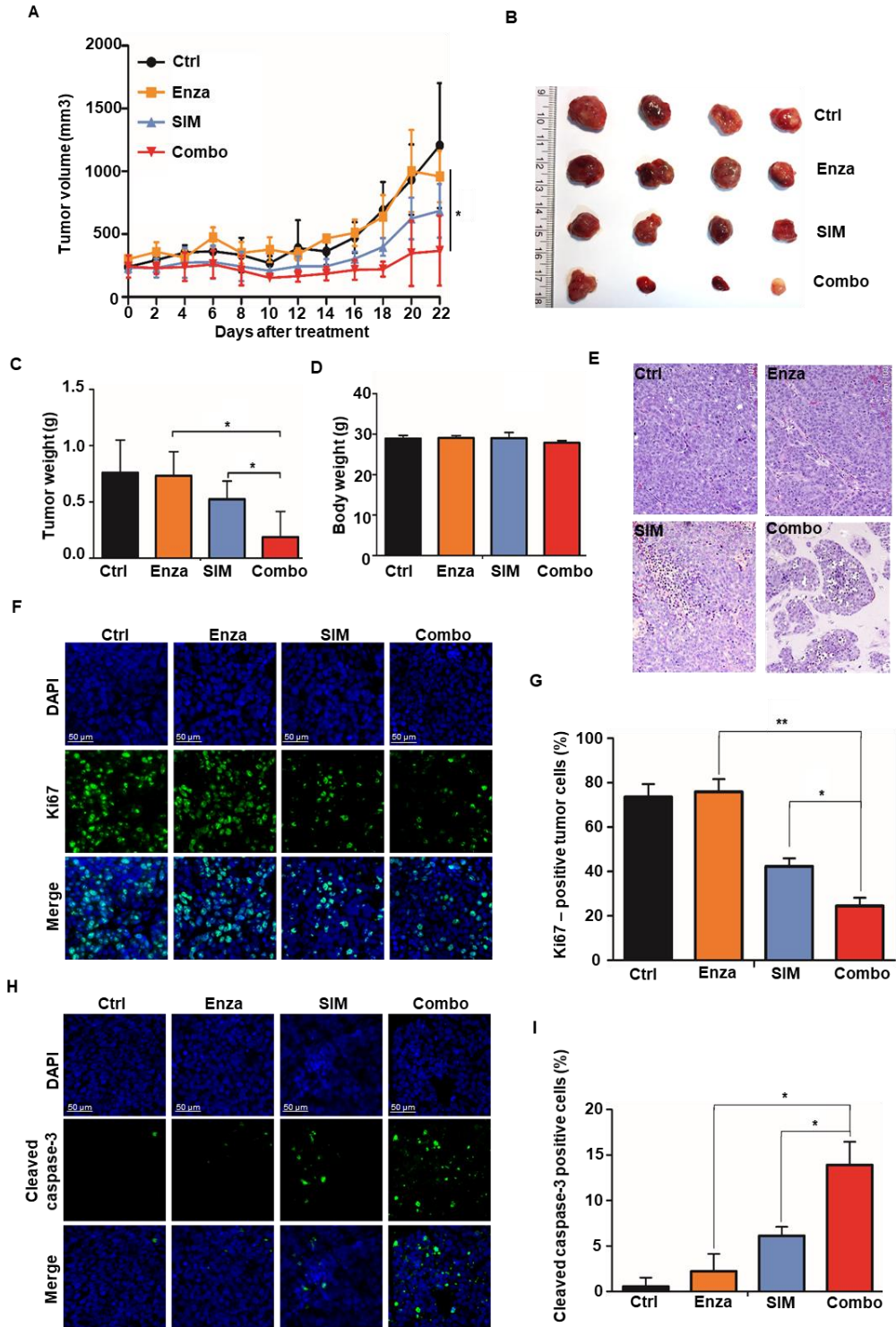
Figure 4. Simvastatin treatment overcomes enzalutamide resistance in vivo

(A-D) Mice bearing 22Rv1 tumors were treated with simvastatin, enzalutamide or the combination
of two drugs as described in Materials and Methods. After 4 weeks, tumors are harvested. Tumor

volumes were measured every 2 days (results are presented as mean ± SD; n = 4 mice in each group). Mice were weighed before sacrifice. Fresh tumors were weighed after sacrifice. **, P < 0.01. (E) Representative images of H&E staining on formaldehyde-fixed, paraffin-embedded 22Rv1 xenograft tumor sections. (F and H) Representative images of anti-cleaved caspase 3 and anti-Ki67 immunofluorescence staining of tumor sections. (G and I) Quantification of Ki67 and cleaved caspase 3 staining. *, P<0.05. **, P<0.01.
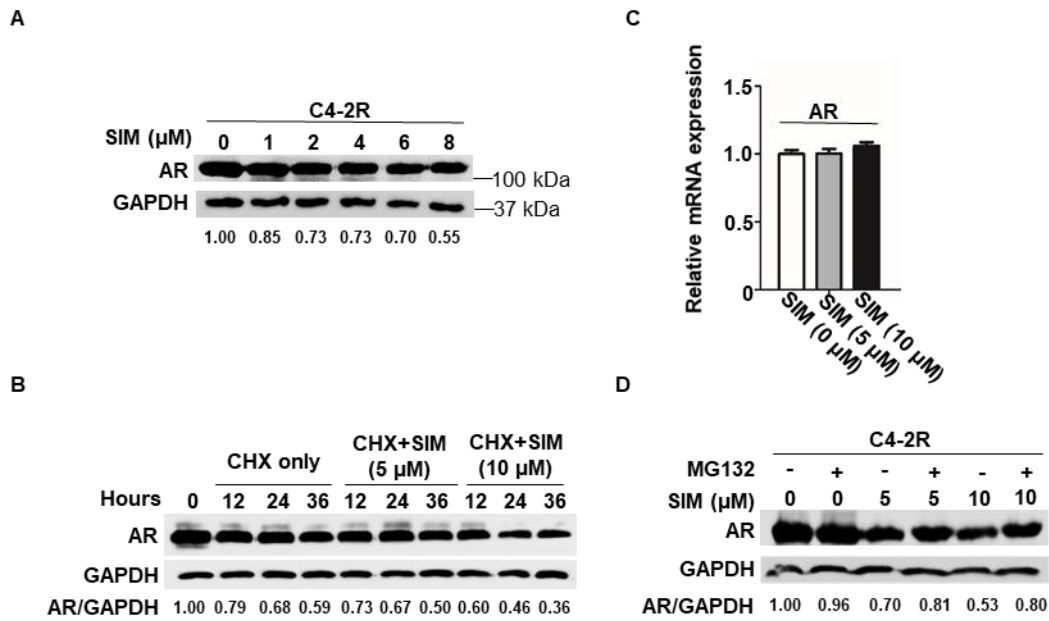
Figure 5. Simvastatin treatment suppresses AR protein level

(A) C4-2R was treated with simvastatin at the indicated concentrations for 2 days, followed by IB against AR and GAPDH. (B) Cells were treated with simvastatin at the indicated concentrations for 2 days and harvested for quantitative RT-PCR. (C) C4-2R cells were treated with simvastatin at the indicated concentrations and 50 µg/ml cycloheximide (CHX), followed by IB against AR. (D) C4-2R cells were treated simvastatin at the indicated concentrations for 48 hours, further incubated with MG132 (5 µM) for 8 hours, and harvested for IB against AR and GAPDH.

A C4-2R

Enza (20µM)	-	+	-	-	-	+	+	+
SIM (µM)	0	0	2.5	5	10	2.5	5	10
AR								
PSA								
GAPDH								
AR/GAPDH	1.00	1.01	0.88	0.71	0.66	0.48	0.61	0.29
PSA/GAPDH	1.00	0.56	3.31	3.31	2.88	0.52	0.53	0.26

B 22RV1

Enza (20µM)	-	+	-	-	-	+	+	+
SIM (µM)	0	0	1	2.5	5	1	2.5	5
AR								
AR-Vs								
GAPDH								
AR/GAPDH	1.00	0.78	0.61	0.58	0.51	0.48	0.43	0.33
AR-V/GAPDH	1.00	0.81	0.39	0.31	0.29	0.22	0.03	0.03

C MR49F

Enz(10µM)	-	+	-	+	-	+
SIM(µM)	-	-	1	1	2.5	2.5
AR						
PSA						
β - Actin						
AR/β-Actin	1.00	0.65	0.65	0.63	0.30	0.11
PSA/β-Actin	1.00	1.10	0.75	0.73	0.32	0.20

D

	MR49F neo	MR49F AR	C4-2R neo	C4-2R AR	22RV1 neo	22RV1 AR
Enza	+	+	+	+	+	+
SIM	+	+	+	+	+	+
AR						
C-PARP						
GAPDH						
AR/GAPDH	1.00	3.36	1.00	3.25	1.00	2.50
C-PARP/GAPDH	1.00	0.75	1.00	0.66	1.00	0.78

E

	Ctrl		HMGCR-KD		
Enza	-	+	-	+	
HMGCR					—100 kDa
	1.00	1.41	0.23	0.40	
AR					—100 kDa
	1.00	1.29	0.84	0.28	
PSA					—37 kDa
	1.00	0.35	1.12	0.18	
β-Actin					—37 kDa

Figure 6. The combination of enzalutamide and simvastatin further decreases AR protein level

(A) C4-2R was treated with enzalutamide (20µM), simvastatin at the indicated concentrations or various combinations of the two drugs for 48 hours, followed by IB against AR and PSA. (B) 22Rv1 was treated with enzalutamide (20µM), simvastatin at the indicated concentrations or various combinations of the two drugs for 48 hours, followed by IB against AR. (C) MR49F was treated with enzalutamide (10µM), simvastatin at the indicated concentrations or different combinations of the two drugs for 48 hours, followed by IB against AR and PSA. (D) C4-2R, MR49F, and 22Rv1 were transiently transfected with AR or pcDNA3.0 as control, cultured in medium with the combination of enzalutamide (20µM) and simvastatin (5µM) for 48 hours, then harvested for western blot against AR and cleaved PARP. (E) Indicated cells were treated with enzalutamide (20µM) or DMSO for 48 hours, and harvested for western blot to test AR, cleaved PARP, and β-Actin.
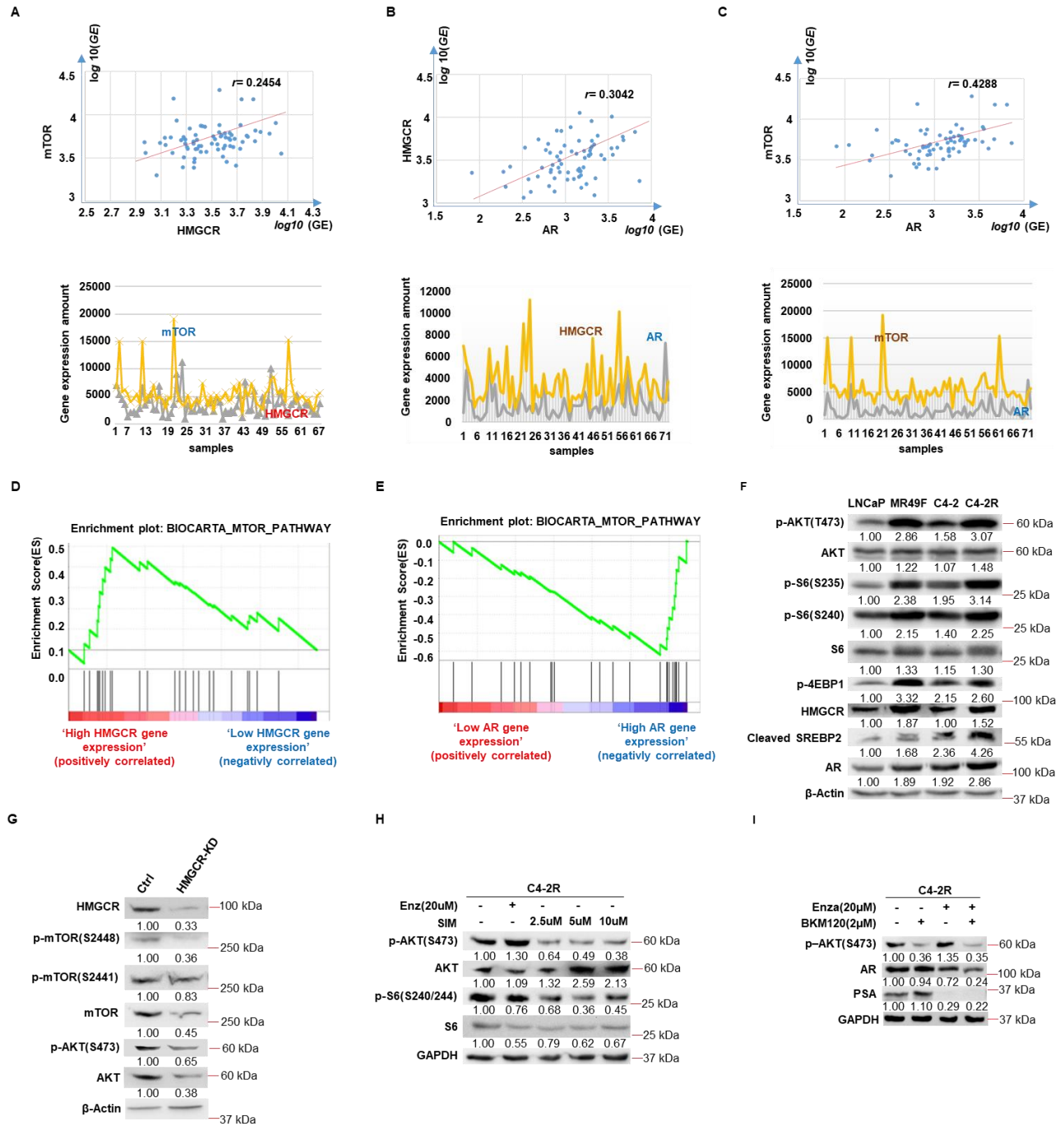
Figure 7. Gene expression of mTOR pathway coreelated with HMGCR and AR expression

(A) Correlation between HMGCR and mTOR expression. (B) Correlation between AR and HMGCR expression. (C) Correlation between AR and mTOR expression. (D) GSEA shows that mTOR pathway gene set is enriched in high-AR group. The enrichment plot shows the distribution

of genes in the set that are correlated with AR expression. (E) GSEA identifies that mTOR pathway gene set is enriched in high-HMGCR group. The enrichment plot shows the distribution of genes in the set that are correlated with HMGCR expression. (F) Indicated cells were cultured in RPMI-1640 media for 48 hours, and harvested for IB. (G) C4-2R was treated with enzalutamide and simvastatin at indicated concentrations for 48 hours, followed by IB. (H) C4-2R was treated with enzalutamide (20uM) or simvastatin at indicated concentrations, followed by IB. (I) C4-2R was treated with enzalutamide and BKM120 at indicated concentrations for 48 hours, followed by IB.

CHAPTER 4. INHIBITION OF EZH2 ENHANCES THE ANTITUMOR EFFICACY OF METFORMIN IN PROSTATE CANCER

4.1 Introduction

Metformin (N, N-dimethylbiguianide), the most commonly used oral drug to treat type II diabetes, has a good safety profile and limited side effects. Increasing observational and cohort studies have shown that diabetes patients who were treated with metformin usually exhibited lower risk of cancer (22), indicating that it is feasible to repurpose metformin as an anti-cancer drug. In PCa, metformin was observed to reduce PCa incidence and slow down the development of CRPC (23, 24). Moreover, a phase II trial observed prostate-specific antigen (PSA) secretion was decreased by the use of a high-dose metformin in progressive metastatic CRPC (25). Recently, a population-based cohort study showed encouraging results that metformin use after diagnosis of PCa might increase survival of patients (26). All of these suggest that metformin could be a useful medication for PCa therapy, but more studies are still needed to further evaluate such a notion.

Enhancer of zeste homolog 2 (EZH2), the catalytic subunit of Polycomb Repressive Complex 2 (PRC2), suppresses expression of a number of genes via catalyzing histone-3 lysine 27 trimethylation (H3K27me3) (27). Accumulating evidence has shown that EZH2 plays an important role in tumor oncogenesis and progression (28). GSK126 (GSK2816126) (80) is an S-adenosyl-methionine-competitive inhibitor targeting EZH2, and it has recently been shown effective and well tolerated in lymphoma (29). However, EZH2 also acts independently of its methyltransferase activity. For instance, EZH2 can activate nuclear factor κB by forming a complex with RelA and RelB, in which methylation isn't involved (30). In PCa, EZH2 can increase AR's expression by binding to its promoter, which is also methylation-independent (31). Therefore, although several EZH2 methyltransferase inhibitors, including GSK126, are proved effective, suppression of EZH2's protein level by drugs should be considered to enhance therapy targeting EZH2.

In our study, we found that the combination of metformin and GSK126 exerts a synergistic anti-proliferative effect in PCa cell lines and in human prostate tumor explants. Furthermore, we demonstrate that metformin can induce downregulation of EZH2 via upregulating miR-26a-5p in LNCaP. Although metformin's role was strongly hampered by the interaction between androgen

receptor (AR) and EZH2 in 22Rv1, it can be restored when combined with GSK126. All of these suggest that the combination of metformin and GSK126 is effective, and acts, at least partially, through inhibition on both EZH2's expression and methyltransferase activity.

4.2 Results

4.2.1 Metformin and GSK126 synergistically inhibit growth of PCa cells

To investigate whether metformin and GSK126 act synergistically to inhibit the growth of PCa cells, colony formation assay was conducted with LNCaP, 22Rv1 and RWPE-1. Compared with treatment of metformin or GSK126 alone, the combination of two drugs exerted a stronger inhibitory effect on colony formation by LNCaP and 22Rv1 (Figs. 8A and 8B), but not the colony formation by RWPE-1 (Fig. 8C), a non-transformed prostate epithelial cell line. In comparison with mono-treatments, the combination of metformin and GSK126 also led to a greater inhibitory effect on cell survival of LNCaP and 22Rv1 (Figs. 8D and 8E), but RWPE1 cells were not affected (Fig. 8F). Moreover, the role of apoptosis was investigated upon different treatments. In LNCaP, the treatment with metformin or GSK126 as a single agent could induce slight apoptosis, but no combinational effect was observed (Figs. 8G). In contrast, neither metformin nor GSK126 alone induced apoptosis in 22Rv1, but there was a dramatic increase of apoptosis induced by the combination (Figs. 8H). Finally, CIs were measured to determine the types of drug interactions. As shown in Figs. 8I and 8J, the combinations exhibited slight to moderate synergy in LNCaP (CI range, 0.87 – 0.72), and moderate to strong synergy in 22Rv1 (CI range, 0.67 – 0.33). Altogether, these results demonstrate that the combination of metformin and GSK126 exerts synergistic inhibitory effect on PCa cell growth.

4.2.2 Metformin is capable to suppress EZH2 expression in PCa cells

Increasing evidence shows that EZH2 is usually upregulated in PCa, and closely associated with progression, invasion and metastasis (81, 82). Therefore, we were prompted to investigate the role of EZH2 in the anti-proliferative effect induced by the treatments. As shown in Fig. 9A, metformin alone significantly suppressed EZH2's expression in androgen-sensitive LNCaP cells, and notably, the combined treatment resulted in enhanced inhibition on EZH2's activity indicated by the level of H3K27me3. In contrast, 22Rv1 cells, which are androgen-independent, displayed a limited reduction of EZH2 when treated with metformin alone, but it was decreased significantly by co-treatment of metformin and GSK126 (Fig. 9B), indicating that GSK126 restored metformin's ability of downregulating EZH2. To further explore how EZH2 was degraded, the relative mRNA

level was measured by qRT-PCR. Consistently, metformin alone significantly reduced EZH2 mRNA level in LNCaP (Fig. 9C), but the combination of metformin and GSK126, instead of mono-treatments, was required to decrease EZH2 mRNA level in 22Rv1 cells (Fig. 9D). It is worthy noticing that the EZH2 expression displayed a similar changing trend with the cell growth upon indicated treatments in both cell lines, so we wondered whether the growth inhibition of PCa cells is indeed due to EZH2 reduction. To test this hypothesis, we expressed exogenous EZH2 in LNCaP and 22Rv1, and then treated them with indicated drugs. We found that overexpression of EZH2 partially rescued the cells from the growth inhibition induced by the treatments (Figs. 9E and 9F). In summary, these results indicate metformin-induced downregulation of EZH2 expression is antagonized in 22Rv1 cells, but such an ability can be restored by co-treatment with GSK126. Also, downregulation of EZH2 is one of the reasons contributing to the anti-proliferative effect induced by the treatments.

4.2.3   Metformin suppresses EZH2 expression via upregulating miR-26a-5p

Next, we aimed to further dissect the underlying mechanism for metformin-mediated EZH2 downregulation. Metformin has been reported to target a variety of microRNAs (83, 84), and some of them, including miR-26a, miR-101, let-7a, let-7b and let-7c, directly regulate EZH2 expression in PCa (85). To examine whether these microRNAs are responsible for metformin-induced inhibition on EZH2's expression, RT-PCR was used to determine their expression levels in LNCaP treated with metformin. As shown in Figs. 2G and 2H, metformin, instead of GSK126, enhanced the expression of miR-26a-5p and miR-101-3p. However, LNCaP cells treated with metformin exhibited decreased expression levels of let-7a-5p, let-7b-5p and let-7c-5p (Fig. 9I), which could not explain metformin-induced EZH2 downregulation. To further verify these observations, LNCaP cells were transfected with miRNA inhibitors, which are small, double-stranded RNA molecules designed to inhibit specific mature miRNAs, and then treated with metformin. As shown in Fig. 9J, metformin-induced reduction of EZH2 was restored by miR-26a-5p inhibitor, but not by the inhibitors targeting miR-101-3p (Fig. 9K), let-7a-5p, let-7b-5p and let-7c-5p (Fig. 9L), indicating that miR-26a-5p is the mediator of metformin-induced EZH2 downregulation. Moreover, the miR-26a-5p level was also assessed in 22Rv1 upon indicated treatments, and we found that although metformin alone failed to upregulate miR-26a-5p, the combined treatment

enhanced it (Fig. 9M). To further validate this finding, we applied the miRNA inhibitor to block the function of miR-26a-5p. We found that the reduction of EZH2 expression level induced by the combination treatment was restored upon addition of miR-26a-5p inhibitor (Fig. 9N). Also, as EZH2 increased, more 22Rv1 cells survived upon the combination treatment (Fig. 9O). Collectively, we conclude that metformin-induced downregulation of EZH2 is through upregulating miR-26a-5p in LNCaP and 22Rv1.

4.2.4 Metformin-induced EZH2 downregulation is affected by AR

To investigate which factors regulates metformin's effect on EZH2 level in PCa cells, we compared the responses to metformin in several PCa cell lines, including PC3, DU145, LNCaP and 22Rv1. As indicated, the low-concentration metformin was capable to significantly decrease EZH2 protein levels in PC3 and DU145 (Figs. 10A and 10B), both of which are AR negative. In LNCaP, which is AR positive and androgen sensitive, metformin inhibited EZH2 expression as well, but with a lower inhibition efficiency (Fig. 10C). However, metformin failed to reduce EZH2 of 22Rv1, which is AR positive and androgen-refractory (Fig. 10D). Since AR, as well as its cofactors, plays a key role in PCa progression and acquisition of drug resistance, we hypothesized that AR might impede metformin's ability of downregulating EZH2. To test this hypothesis, we assessed the effect of synthetic androgen (R1881) stimulation of AR on EZH2 expression upon metformin treatment. As shown in Fig. 10E, EZH2 protein level was significantly decreased by metformin, accompanied by a reduction of AR activity in LNCaP. However, metformin-induced downregulation of EZH2 in LNCaP was partially restored by addition of R1881. Meanwhile, we also detected the level of miR-26a-5p, and found that treatment of LNCaP with R1881 significantly abolished metformin induced re-expression of miR-26a-5p (Fig. 10F). To further confirm this, two engineered PC3 cell lines were used. PC3-AR contains the coding region of human AR and stably expresses it, while PC3-Neo contains the same vector without the AR cDNA sequence. PC3-AR and PC3-Neo cells were treated with metformin, followed by western blot to determine EZH2 protein levels. As shown in Fig. 10G, PC3-Neo, rather than PC3-AR, displayed a remarkable decreasing trend of EZH2 expression as metformin concentration increases. Accordingly, miR-26a-5p was upregulated upon the treatment of metformin in PC3-Neo, but not in PC3-AR (Fig. 10H). Finally, we constructed two 22Rv1 cell lines with stable knockdown of AR, and treated

them with metformin. As expected, depletion of AR led to a significant decrease of EZH2 protein level (Fig. 10I) and an increase of miR-26a-5p in response to metformin treatment (Fig. 10J), further supporting the notion that AR affects metformin-induced EZH2 downregulation.

4.2.5   AR directly suppresses miR-26a transcription by binding to its promoter

Next, we investigated whether AR could bind to the promoter of miR-26a-5p and directly regulate its expression in PCa cells. After assessing the 2-kb region of genomic DNA upstream of miR-26a-5p using PROMO, we identified eight potential binding motifs for AR lying within -1955 to -1903, -1136 to -1128, -488 to -449 regions on chromosome 3, and -189 to -12 regions on chromosome 12 (Fig. 11A). To examine whether AR could physically bind to the promoter of miR-26a-5p, chromatin immunoprecipitation (ChIP)-PCR assays were performed in 22Rv1 and LNCaP. Two AR-binding sites, P1 and P2, of miR-26a-5p promoter regions exhibited significant enrichment upon immunoprecipitation with the AR antibody, but no bands were evident for other two sites, P3 and P4 (Fig. 11B). We then sub-cloned the promoter region including both P1 and P2 upstream of luciferase gene into a reporter plasmid. The dual-luciferase assay showed that the transcriptional activity was reduced when AR bound to the sites, and treatment of R1881 further decreased it (Figs. 11C and 11D), indicating that AR binds to the promoter of miR-26a-5p and inhibits its expression as predicted. Furthermore, we asked whether metformin and GSK126 affected the AR binding to the promoter of miR-26a-5p. As shown in Figs. 11E and 11F, either metformin or GSK126 alone reduced the AR binding to the promoter within limited extent, but the combination of metformin and GSK126 almost completely removed AR from the regions.

It is well known that metformin can reduce AR recruitment to the promoters of its target genes (86), but we asked how GSK126 could also reduce it. Recently, EZH2 was shown to interact with AR to regulate its binding to its target genes, in a manner dependent on EZH2's methyltransferase activity (87). In addition, the interaction between AR and EZH2 is mediated by phosphorylation at S21 of EZH2 (87). Therefore, we further hypothesized that AR cooperates with EZH2 to suppress miR-26a-5p expression. To test this, the miR-26a promoter construct was co-transfected with empty vector, AR, EZH2-S21D and EZH2-S21A either alone or in combination with AR plus EZH2-S21D and AR plus EZH2-S21A in HEK293T cells. We found that EZH2-S21D, instead of

EZH2-S21A, promoted AR's inhibition on the transcriptional activity (Fig. 11G), suggesting that EZH2 interacts with AR to regulate the expression of miR-26a-5p. To further validate this point, re-ChIP assay was performed, and revealed that AR, bound to the miR-26a-5p promoter region, was significantly associated with EZH2 in 22Rv1 cells (Fig. 11H), but not in LNCaP cells (Fig. 11I). Altogether, these results suggest that expression of miR-26a-5p was suppressed by AR in PCa cells, and that the AR/EZH2 complex reinforced the suppression in advanced androgen-refractory PCa cells.

4.2.6 Metformin and GSK126 act synergistically in a 22Rv1-derived xenograft model

To further validate our in vitro finding, we evaluated the effect of metformin and GSK126 alone or in combination with a 22Rv1-derived xenograft mouse model. After a 24-day treatment, we found that metformin alone could barely affect the tumor growth, and GSK126 alone only exerted a limited inhibitory effect on it (Figs. 12A-C). In contrast, the combination of metformin and GSK126 significantly blocked the tumor growth and decreased the tumor weight. Meanwhile, no significant body weight loss was observed among all four groups (Fig. 12D), implying that the combination of the two drugs with the indicated doses has little toxic side effect. To confirm the responses, we conducted histological analyses of these tumor samples. H&E staining showed that single agent metformin, as well as GSK126, slightly reduced the tumor cell content (Fig. 12E); however, tumor cell content was markedly decreased after the combination therapy with metformin and GSK126 (Fig. 12E). Furthermore, the immunostaining of Ki67 and cleaved caspase-3 also showed that the combination of metformin and GSK126 led to a significant decrease in overall proliferation and a dramatic increase of apoptosis (Figs. 12F-I). Finally, proteins were extracted from the harvested tumors and subjected to western blot against EZH2. We also found that co-therapy of metformin and GSK126 significantly lowered EZH2 expression than the mono-therapies (Figs. 12J-L). These results are consistent with what we observed in the cell-based experiments, thus confirming the synergistic effect between metformin and GSK126.

4.2.7 Metformin and GSK126 act synergistically in a patient-derived xenograft model

To better mimic the growth and situation of CRPC, a patient-derived xenograft study was conducted by using of LuCaP35CR, which could represent the major genomic and phenotypic features of the disease in humans. As predicted, the combination of GSK126 and metformin resulted in a more pronounced tumor-inhibitory effect than did monotherapies (Figs. 13A-C). Also of note, the serum PSA, which is often elevated with the progression of PCa, displayed significant reduction upon the combination treatment (Fig. 13D). Moreover, histological analyses of these tumors showed that there was not a significant difference between control group and metformin group. GSK126-treated tumors exhibited some apoptotic bodies and morphological changes including cytoplasm reduction, nuclear pyknosis and karyorrhexis (Fig. 13E). Remarkably, the tumors treated with both metformin and GSK126 showed increasing number of apoptotic bodies with pyknotic or fragmented nuclei, as well as condensed cytoplasm (Fig. 13E). Immunostaining of Ki67 and cleaved caspase-3 also revealed that the combination of metformin and GSK126 led to a significant decrease in overall proliferation and a dramatic increase of apoptosis (Figs. 13F-I). Finally, we also analyzed EZH2 protein levels in all the tumor samples, and found that co-treatment of metformin and GSK126 led to a lower expression of EZH2 compared with either drug alone (Figs. 13J-L). In summary, these results are consistent with that of 22Rv1-derived xenograft study, further confirming that metformin and GSK126 can act synergistically in CRPC.

4.3 Discussion

Currently, there are no curative therapies for CRPC, and novel therapeutic methods are urgently needed. In our study, we investigated whether metformin and GSK126 could be combined for treatment of PCa. We investigated the potential of metformin plus GSK126 based on the hypothesis that their different inhibitory effects on EZH2 could combine to exert a synergistic anti-tumoral effect.

We demonstrated that the combination of metformin and GSK126 synergistically inhibited proliferation of LNCaP and 22Rv1, but not RWPE1. Compared with LNCaP, we noticed that the combination is more synergistic in 22Rv1; meanwhile, 22Rv1 is much more resistant to metformin, suggesting that GSK126 strongly enhances the potency of metformin and re-sensitizes 22Rv1 to it. Previous studies of our laboratory also showed that different PCa cells have different sensitivities to metformin, and advanced AR-positive PCa cells are usually resistant (88, 89), which is in agreement with our finding in this study. Similar to most malignancies, prostate tumors are usually composed of multiple cell types, with complexed characteristics and biological features, resulting in intra-tumoral heterogeneity; therefore, it seems that metformin is not a promising anti-cancer monotherapy for CRPC, and combinations of metformin with other drugs potentiating its function should be more viable.

It has been well documented that EZH2 is critical for PCa growth, development and progression (28). Recent studies revealed EZH2 could act independently of its methyltransferase activity (31), indicating additional approaches inhibiting EZH2 expression should also be considered. In our study, metformin could downregulate EZH2 through upregulating miR-26a-5p in LNCaP, but not in 22Rv1. Considering that 22Rv1 is more resistant to metformin than LNCaP, we aimed to dissect the underlying mechanism. We found that metformin's effect on EZH2 was actually antagonized by AR, which impeded metformin-induced re-expression of miR-26a-5p, and modification of AR changed metformin's effect on EZH2. We also noticed that metformin could decrease EZH2 by eliminating AR's inhibitory effect on miR-26a-5p in LNCaP, but it could also reduce EZH2 in PC3 and DU145 as well, indicating that additional molecules besides AR are involved in metformin's regulation on EZH2.

It has been reported AR could inhibit gene expression by directly binding to its promoter (90). Also, previous studies showed that AR could directly bind to the promoters of miRNAs to regulate their expression (91, 92). Consistently with these findings, we observed AR bound to the promoter of miR-26a and suppressed its expression. Furthermore, we proved that the gene inhibition induced by AR could be reinforced by EZH2-S21D, which is consistent with previous research demonstrating that EZH2 promoted AR recruitment to its sites via directly methylating it (87, 93). Also, we found that GSK126 decreased AR's recruitment at the promoter of miR-26a, further supporting the interaction between AR and EZH2 we observed.

We also tested the combination of the two drugs by in vivo experiments, and found it could inhibit tumor growth, induce apoptosis, and downregulate EZH2 in both 22Rv1-derived tumors and LuCaP35CR xenografts. Meanwhile, the dosage we used did not cause any toxic effect. The safe dosage of metformin for patients should be below 3,000 mg per day (94, 95). The dosage used in our mice experiments is 30 mg/kg body weight/day, which is within safe medication range. In the phase I study, GSK126 was escalated to maximum dose of 3,000 mg twice a week for patients with no dose limiting toxicity observed (29). However, the dosage used in our experiments is 50 mg/kg body weight/day, which was slightly higher and more frequent than the dosage in the clinical trial. Till now, the safety limit of GSK126 is still undetermined, so our results are valuable to define the appropriate dosage range of medication of GSK126 for clinical use.

In summary, as shown in Fig. 13M, miR-26a-5p is negatively regulated by AR in LNCaP, which can be easily eliminated by metformin. Moreover, EZH2 reinforces AR's inhibition on miR-26a-5p expression in 22Rv1, which results in the resistance. However, inhibition of EZH2's methyltransferase activity with GSK126 can inhibit the interaction between AR and EZH2, restoring metformin's effect in 22Rv1. Therefore, our results suggest that the combination of metformin and GSK126 would be an effective approach targeting EZH2 for future PCa therapy, in particular, for AR-positive CRPC patients.
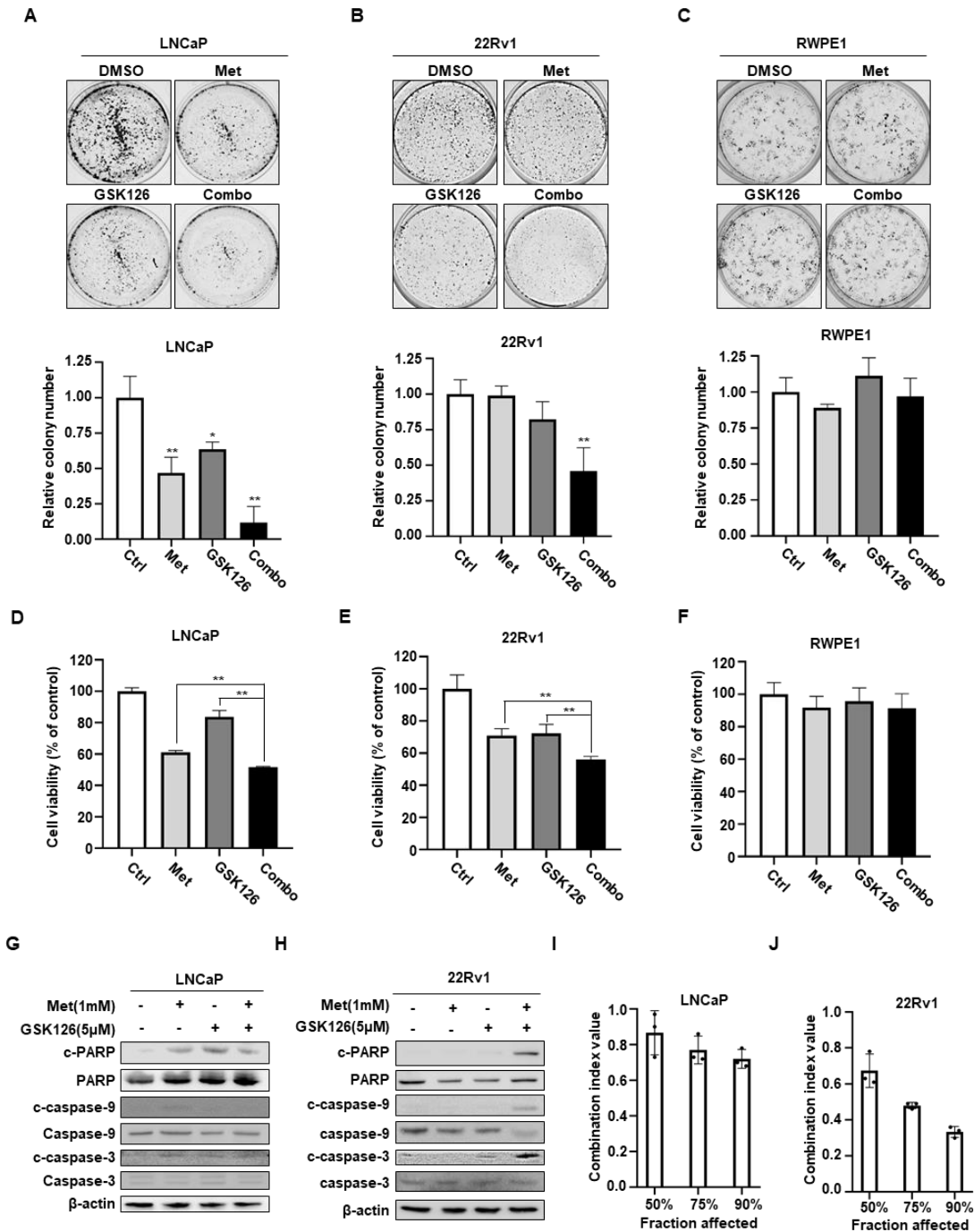
Figure 8. Metformin and GSK126 in combination synergistically inhibit growth of PCa cells.

(A - C) LNCaP, 22Rv1 or RWPE1 cells were plated into 6-well plates, and treated with metformin (0.5 mM), GSK126 (2.5 µM), or both for 12 days, followed by crystal violet staining to monitor colony formation. Data shown are representative of data from three repeats. The numbers of

colonies were quantified by using ImageJ software (means ± standard deviations; n = 3 independent experiments). *, P ≤ 0.05; **, P ≤ 0.01. **(D - F)** LNCaP, 22Rv1 or RWPE1 cells were treated with DMSO, metformin (1 mM), GSK126 (5 μM) or both for 72 hours, followed by MTT assay. The results represent the mean of three independent experiments. *, P ≤ 0.05; **, P ≤ 0.01. **(G and H)** LNCaP and 22Rv1 cells were treated with DMSO, metformin (1 mM), GSK126 (5 μM) or both for 48 hours, followed by IB against pro- and cleaved-PARP and caspases. **(I and J)** Combination indice of metformin and GSK126 in 22Rv1 and LNCaP cells.
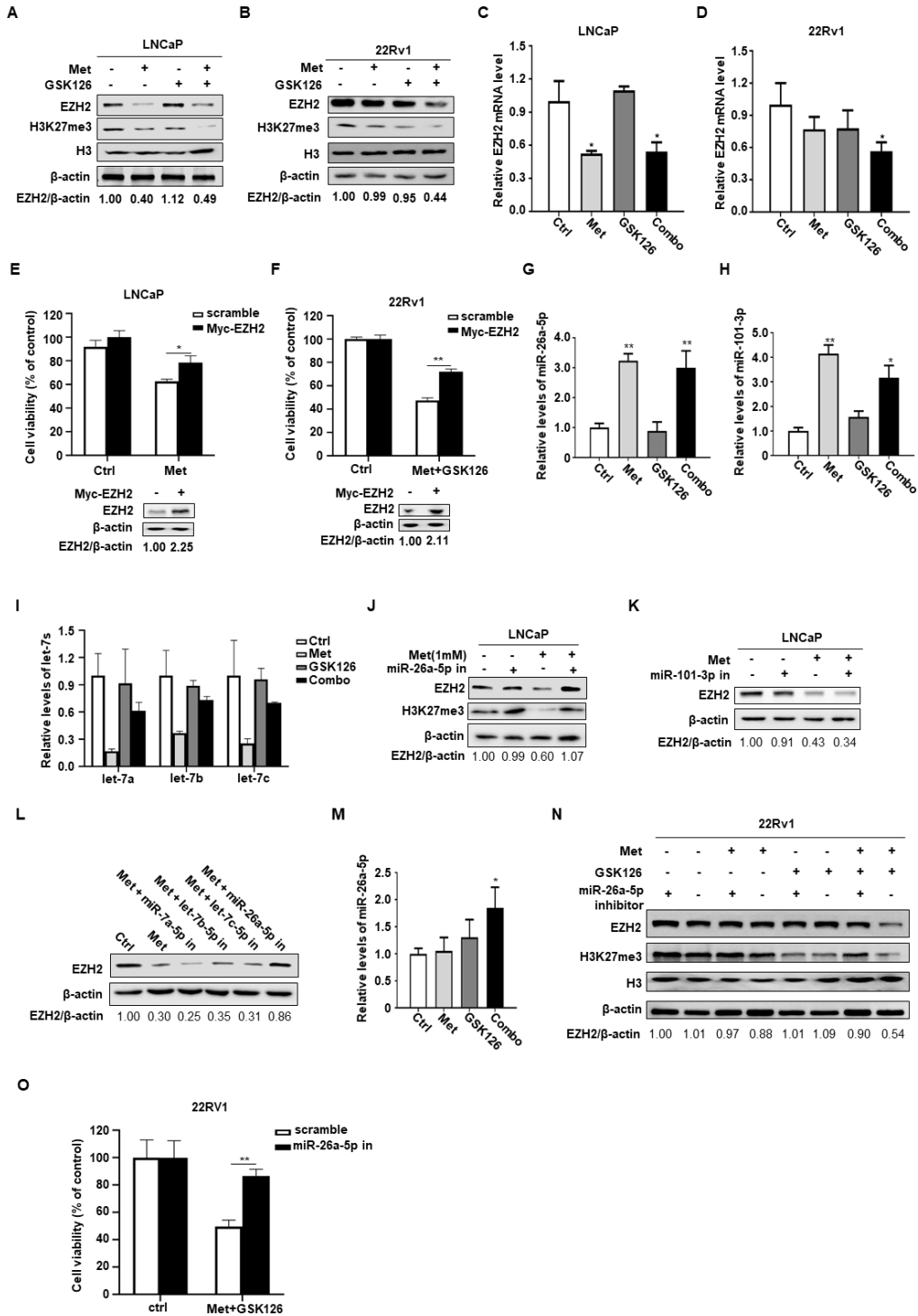
Figure 9. Metformin downregulates EZH2 expression by regulating miR-26a-5p.

(A and B) LNCaP or 22Rv1 cells were treated with DMSO, metformin (1 mM), GSK126 (5 μM) or both for 48 hours, followed by IB. **(C and D)** LNCaP and 22Rv1 cells were treated with

metformin (1 mM), GSK126 (5 µM) or both for 48 hours, followed by qRT-PCR. **(E and F)** LNCaP and 22Rv1 cells were transfected with EZH2 and pcDNA3.0, followed by 72-hour cell viability assay with indicated treatments (metformin: 1 mM; GSK126: 5 µM; means ± standard deviations; n = 3). *, $P \leq 0.05$; **, $P \leq 0.01$. Meanwhile, some cells were harvested for western blot to test EZH2 level after the treatments. **(G - I)** qRT-PCR shows the expression of miR-26a-5p, miR-101-3p, let-7a-5p, let-7b-5p and let-7c-5p of LNCaP cells treated with metformin (1 mM), GSK126 (5 µM) or combination of the two drugs for 48 hours, with all microRNA expressions being normalized to RNU6-2. **(J)** LNCaP cells were transfected with the miR-26a-5p inhibitor or negative control miRNA inhibitor, then treated with metformin (1 mM), GSK126 (5 µM) or both for 48 hours, followed by IB. **(K)** LNCaP cells were transfected with the miR-101-3p inhibitor or the negative control miRNA inhibitor, then treated with metformin (1 mM) for 48 hours, and harvested for IB. **(L)** LNCaP cells were transfected with inhibitors targeting let-7a-5p, let-7b-5p and let-7c-5p or the negative control miRNA inhibitor, then treated with metformin (1 mM) for 48 hours, and harvested for IB. **(M)** qRT-PCR shows the expression of miR-26a-5p of 22Rv1 cells treated with metformin (1 mM), GSK126 (5 µM) or both for 48 hours, with miR-26a-5p expression being normalized to RNU6-2. **(N)** 22Rv1 cells were transfected with miR-26a-5p inhibitor or negative control miRNA inhibitor, then treated with metformin (1 mM), GSK126 (5 µM) or both for 48 hours and harvested for IB. (O) 22Rv1 cells were transfected with miR-26a-5p inhibitor or negative control miRNA inhibitor, treated with DMSO or the combination of metformin (1 mM) and GSK126 (5 µM) for 72 hours, followed by MTT assay (means ± standard deviations; n = 3). *, $P \leq 0.05$; **, $P \leq 0.01$.
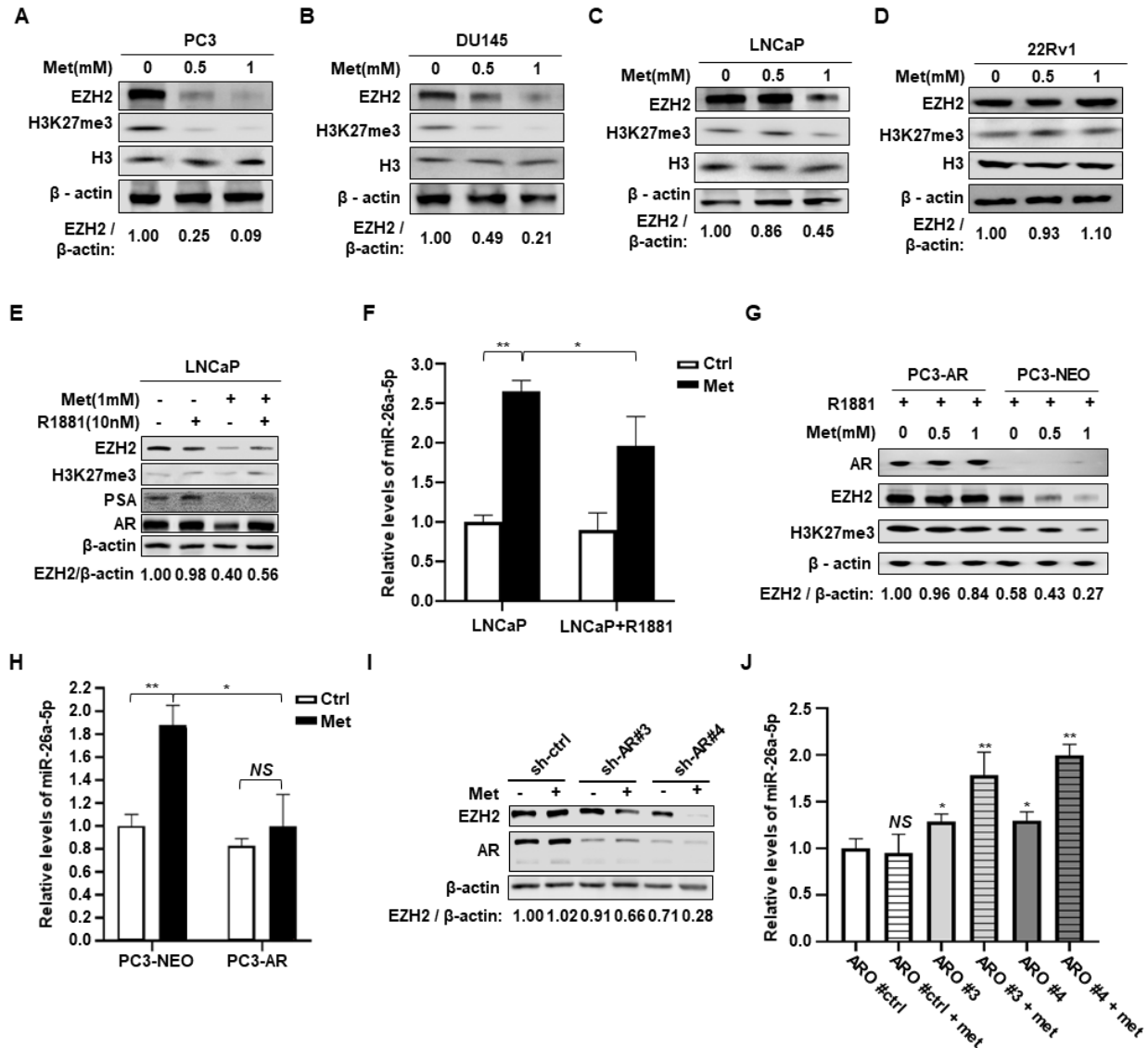
Figure 10. AR affects PCa cells' response to metformin.

(**A - D**) PC3, DU145, LNCaP and 22Rv1 cells were treated with metformin of indicated concentrations for 48 hours, and harvested for IB. (**E and F**) LNCaP cells were treated with 10 nM R1881 or metformin or metformin plus R1881 for 48 hours, followed by IB. Meanwhile, mRNA was extracted for the detection of levels of miR-26a-5p. (**G**) PC3 (-AR or -Neo) cells were treated with metformin of indicated concentrations, as well as 10 nM R1881 to activate AR, and subjected to IB. (**H**) mRNA was extracted from PC3-Neo and PC3-AR cells treated with 1 mM metformin for 48 hours, followed by qRT-PCR to test the levels of miR-26a-5p. (**I and J**) 22Rv1

cells were stably transfected with sh-control, sh-AR #3 and sh-AR #4, and treated with 1 mM metformin for 48 hours, followed by IB to test EZH2 protein level and qRT-PCR to detect miR-26a-5p level.
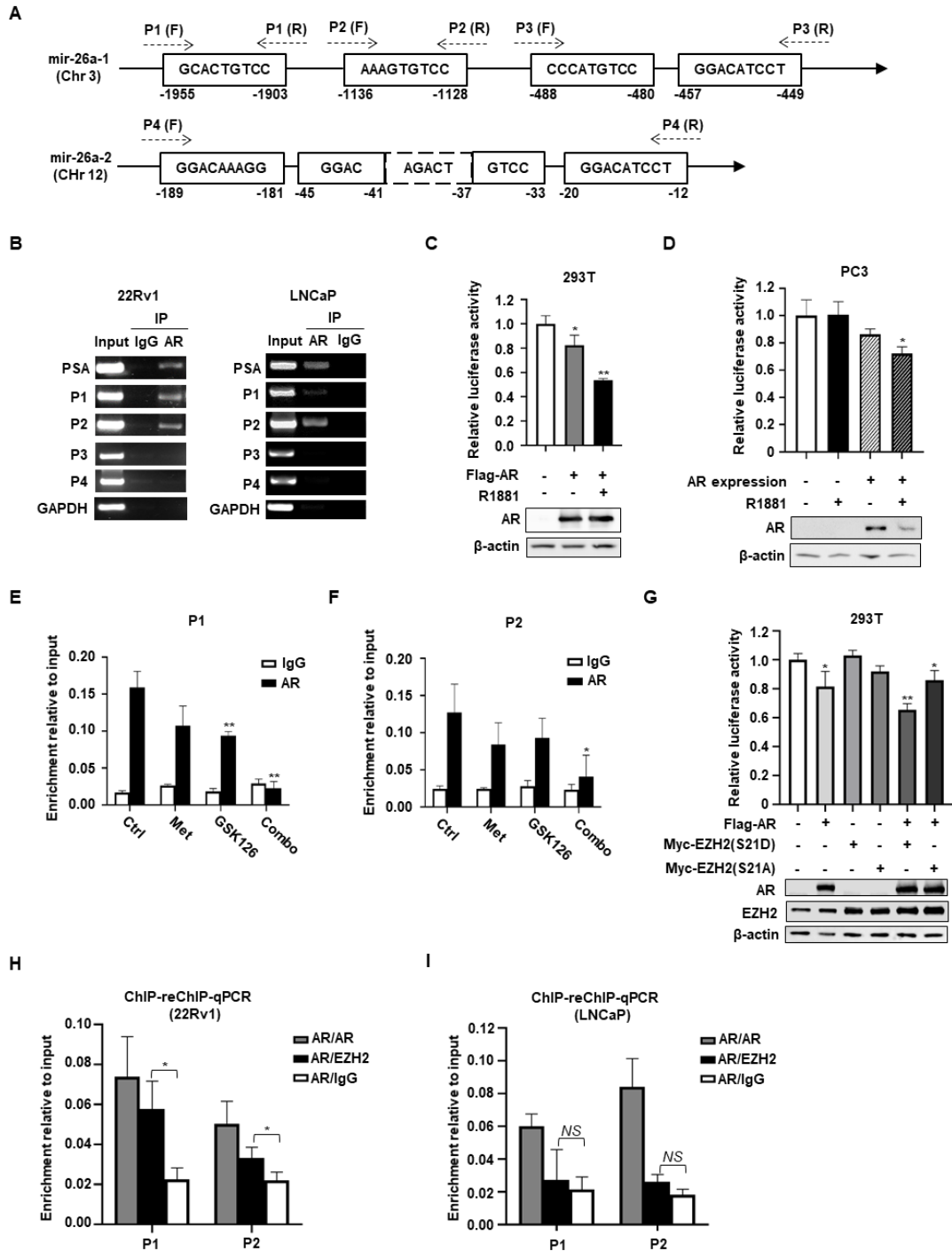
Figure 11. The miR-26a-5p is directly regulated by AR.

(**A**) Scheme representing the binding sequences within the miR-26a promoter relative to the designed primers. (**B**) ChIP analysis of AR binding to the miR-26a promoter region in 22Rv1 and LNCaP cells. (**C and D**) HEK293T cells and PC3-Neo or PC3-AR cells were co-transfected with

the miR-26a promoter construct with empty vector or AR for 24 hours, treated with R1881 (10 nM) for additional 24 hours, and harvested for luciferase assays. Values are means ± standard deviations; n = 3. *, P ≤ 0.05; **, P ≤ 0.01. **(E and F)** 22Rv1 cells were treated with DMSO, metformin (1 mM), GSK126 (5 μM) or both for 48 hours, and harvested for anti-AR ChIP using qPCR to measure the binding of AR to the promoter of miR-26a. Values are means ± standard deviations; n = 3. *, P ≤ 0.05; **, P ≤ 0.01. **(G)** HEK293T cells were transfected with the miR-26a promoter construct in the presence of AR, EZH2-S21D or EZH2-S21A, and harvested for luciferase assays. Values are means ± standard deviations; n = 3. *, P ≤ 0.05; **, P ≤ 0.01. **(H and I)** Chromatin was precipitated with anti-AR antibody, and re-precipitated with anti-AR or anti-EZH2 antibody or IgG, followed by qPCR. Values are means ± standard deviations; n = 3. *, P ≤ 0.05; **, P ≤ 0.01.
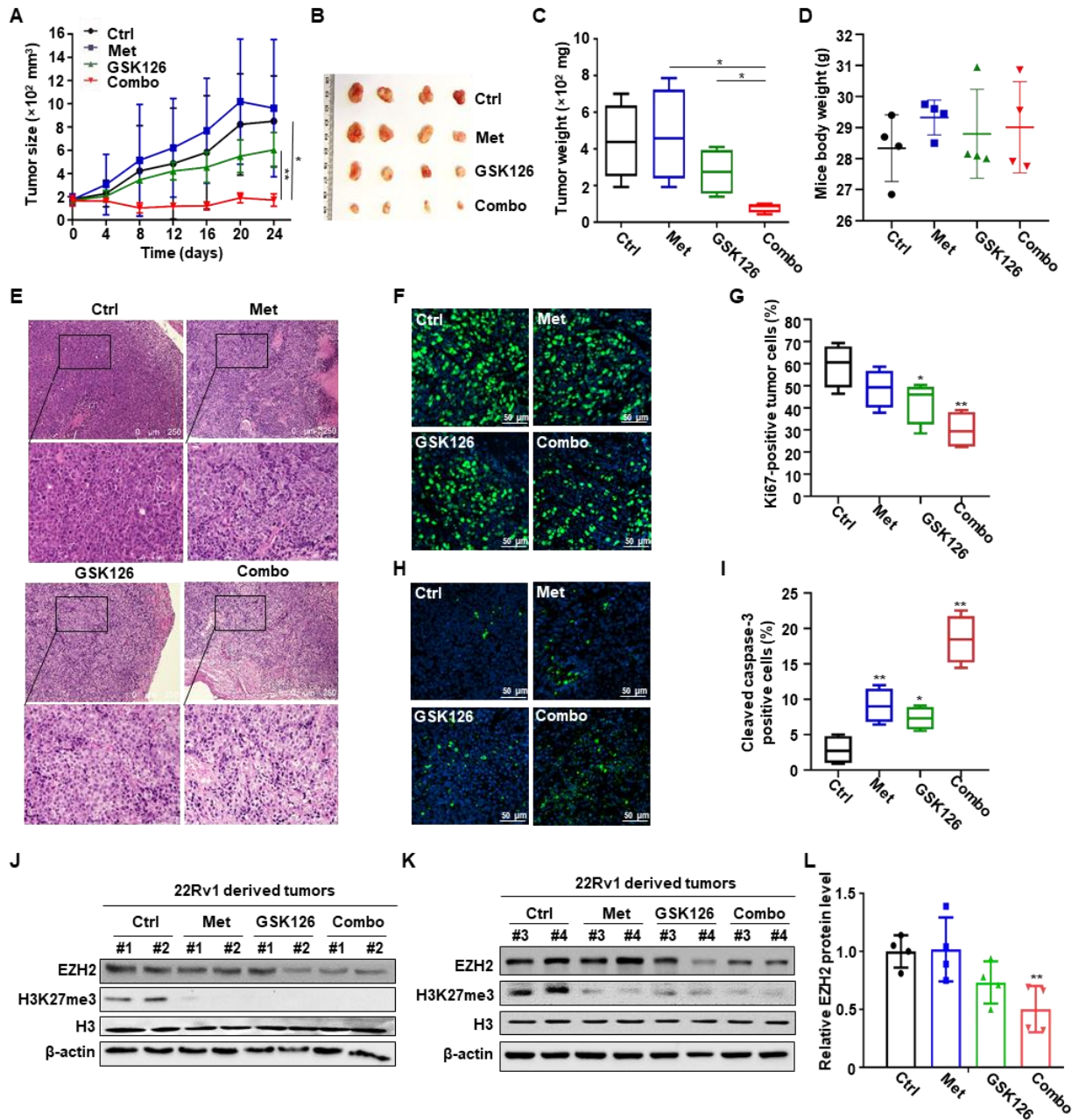
Figure 12. Combination of metformin and GSK126 reduced cell proliferation, increased apoptosis and inhibited EZH2 expression in 22Rv1-derived xenograft tumors.

(**A**) Tumor growth curves of 22Rv1-derived mouse xenografts. After nude mice were innoculated with 22Rv1 cells (2.5×10^5 / mouse) for two weeks, the mice were treated with drugs as described in the method. The sizes of the tumors in each group were measured every 4 days (mean ± S.D.; n=4 mice for each group). *, $P \leq 0.05$; **, $P \leq 0.01$. (**B**) Images of the 22Rv1-derived xenograft

tumors at the end of study. **(C)** Measurement of tumor weight upon harvest. **(D)** Measurement of mice body weight upon tumor harvest. **(E)** Representative images of H&E staining on formaldehyde-fixed, paraffin-embedded, 22Rv1-derived tumor sections. **(F)** Representative images of anti-Ki67 IHC staining of tumor sections. **(G)** Quantification of Ki67 signals as percentages of Ki67-positive cells compared to the total numbers of cells. Multiple tumor sections were calculated (means ± standard deviations; n = 4). *, P ≤ 0.05; **, P ≤ 0.01. **(H)** Representative images of anti-cleaved caspase-3 IHC staining of tumor sections. **(I)** Quantification of cleaved caspase-3 signals as percentages of cleaved caspase-3-positive cells compared to the total numbers of cells. Multiple tumor sections were calculated (means ± standard deviations; n = 4). *, P ≤ 0.05; **, P ≤ 0.01. **(J and K)** Protein lysates extracted from 22Rv1-derived tumors were subjected to western blot for EZH2 and H3K23me3, as well as H3 and β-actin expression. **(L)** Quantification of EZH2 protein levels in J and K.
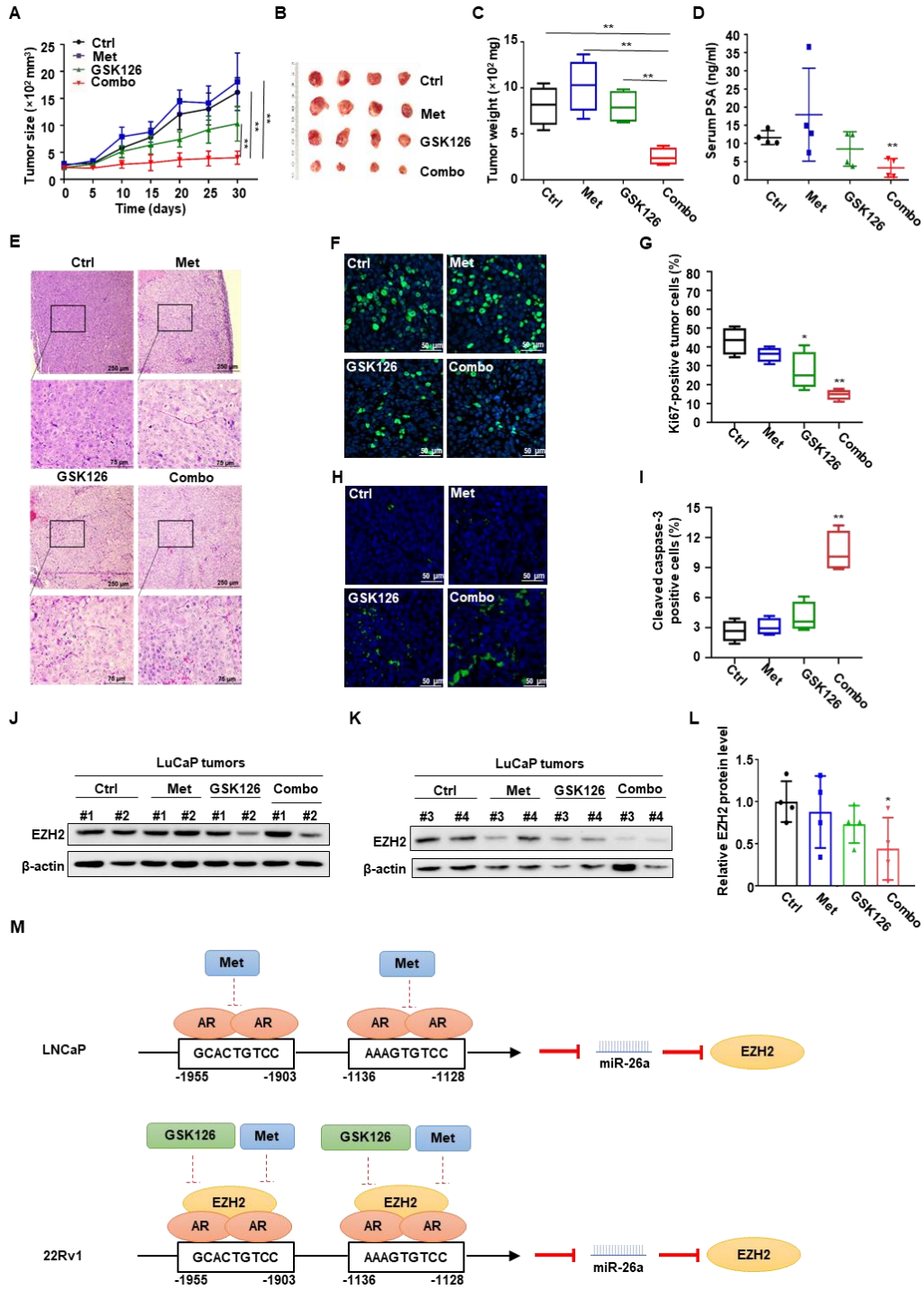
Figure 13. Combination of metformin and GSK126 reduced cell proliferation, increased apoptosis and inhibited EZH2 expression in LuCaP35CR xenograft tumors.

(**A**) Tumor growth curves of LuCaP35CR xenografts (mean ± S.D.; n=4 mice for each group). *, P ≤ 0.05; **, P ≤ 0.01. (**B**) Images of the LuCaP35CR xenograft tumors at the end of study. (**C**)

Measurement of tumor weight upon harvest. **(D)** Blood was collected immediately when the mice were sacrificed, and a PSA enzyme-linked immunosorbent assay kit was used to measure the serum PSA levels. **(E)** Representative images of H&E staining on formaldehyde-fixed, paraffin-embedded, LuCaP35CR tumor sections. **(F)** Representative images of anti-Ki67 IHC staining of tumor sections. **(G)** Quantification of Ki67 signals as percentages of Ki67-positive cells compared to the total numbers of cells. Multiple tumor sections were calculated (means ± standard deviations; n = 4). *, $P \leq 0.05$; **, $P \leq 0.01$. **(H)** Representative images of anti-cleaved caspase-3 IHC staining of tumor sections. **(I)** Quantification of cleaved caspase-3 signals as percentages of cleaved caspase-3-positive cells compared to the total numbers of cells. Multiple tumor sections were calculated (means ± standard deviations; n = 4). *, $P \leq 0.05$; **, $P \leq 0.01$. **(J and K)** Protein lysates extracted from LuCaP35CR tumors were subjected to EZH2 western blotting. **(L)** Quantification of EZH2 protein levels in J and K. **(M)** Proposed working model based on the results of this study.

CHAPTER 5.   PLK1 OVEREXPRESSION PROMOTES DEVELOPMENT OF KRAS[G12D]/TRP53[FL/FL]-DRIVEN LUNG ADENOCARCINOMA

5.1   Introduction

Lung cancer is the leading cause of cancer-related death in the United States, with 228,150 new cases and 142,670 deaths estimated in 2019 (32). Among all cases, non-small-cell lung cancer (NSCLC) amounts for the vast majority. Till now, various molecular targets or oncogenic driver mutations has been identified, including EGFR, ALK, Kras, p53, RET, etc (33). Although drugs designed as inhibitors targeting these molecules has significantly benefited the patients of NSCLC, acquired or de novo resistance often occurs. Therefore, a better understanding of the molecular mechanisms of the disease is needed to discover new molecules to be targeted, as well as to develop more effective therapeutics.

Polo-like kinase 1(PLK1) is a serine/threonine kinase which plays an important role in cell cycle regulation. PLK1 is responsible for mitosis entry (34), spindle assembly (35), kinetochore function (36), centrosome maturation (37), cytokinesis (38), APC/C activity (39), etc. Given the nature of PLK1 and its involvement in mitotic process, much interest has been raised in basic and clinical study of PLK1. PLK1 is reported to be overexpressed in a wide spectrum of human cancers (40). In NSCLC, PLK1 is expressed at higher levels in NSCLC cell lines or tumors compared to normal human bronchial epithelial cell line or non-tumor tissues, and overexpression of PLK1 is correlated with unfavorable patient outcomes (41, 42). Although small-molecule inhibitors targeting PLK1 have been widely studied in in vitro experiments or clinical trials (43), how PLK1 promotes NSCLC still remains unclear.

In this study, we found that elevated levels of PLK1 promoted NSCLC tumor growth launched by classical oncogenic mutations as Kras[G12D] and homozygous loss of P53, and knockout of PLK1 inhibited it. Mechanistically, PLK1 further activated MAPK pathway mainly through increasing gene expression of RET.

5.2   Results

5.2.1   PLK1 overexpression in LADC correlates with poor patient survival

To explore PLK1's role in LADC, a large-scale analysis of PLK1 mRNA expression was firstly performed using data from LADC patients (96). As shown in Fig. 14A, high expression of PLK1 significantly lowered patients' survival, whereas the patients with low PLK1 levels had better survival. Furthermore, high PLK1 expression was significantly correlated with large tumor size (Fig. 14B), as well as poor tumor differentiation (Fig.14C). Taken together, these results indicate that PLK1 overexpression promotes LADC development, and it may also be used as a biomarker of prognosis of lung cancer. Therefore, we are prompted to study the underlying mechanism for PLK1's regulation in LADC.

5.2.2   Modification of PLK1 in KP mouse model

To investigate the contribution of PLK1 to LADC development in vivo, we performed genetic crosses to incorporate a PLK1 overexpressing gene or floxed PLK1 alleles into a KP (Kras^{G12D}; P53$^{fl/fl}$) mouse model that develops LADC (Fig. 15A). PLK1's role was determined primarily through comparison between KPPI and KP, and KPPO was examined in contrast to the KP model to solidify the results of this study. The KP, KPPI and KPPO mice were infected with adenovirus-expressing Cre (Ad-Cre) recombinase via intratracheal instillation (Fig. 15B). PCR and Immunoblotting verified that Rosa-LSL-PLK1 was inserted into the genome of KP mice and expressed successfully (Fig. 15C and D). Following Ad-Cre infection, KPPI mice could develop LADC with PLK1 overexpression (Fig. 15E). Moreover, PLK1$^{flox/flox}$ could also be successfully inserted (Fig. 15F), and PLK1 was eliminated completely after Ad-Cre infection (Fig. 15G). These data definitively show that modification of PLK1 in KP mice was successful, and could be used to study PLK1's roles in KP-initiated LADC.

5.2.3 PLK1 overexpression accelerates development of LADC

Following Ad-Cre infection, we found that KPPI mice developed significantly larger lung tumors than KP mice, with average tumor burden increased from 33.41% for KP mice to 54.36% for KPPI mice (Fig. 16A-C). Also, KPPI mice became moribund earlier, with 91 days of median survival compared with 113.5 days in KP mice (Fig. 16D). Two weeks after MRI imaging, fresh tumors were harvested for further analyses (Fig. 16E). Immunoblot analysis, IHC and immunofluorescence staining verified higher PLK1 protein levels in the tumors from KPPI mice infected with Ad-Cre (Fig. 16F and G). H&E staining confirmed NSCLC (adenocarcinoma) histology of KP tumors, and PLK1 overexpression did not change the histological subtype in KPPI tumors (Fig. 16H). In detail, the WT model showed histologically unremarkable alveolated lung parenchyma with a notable absence of tumor. The alveoli spaces in this model were open and contained thin septa with a single capillary containing red blood cells and small luminal pneumocytes that were flat, lacked an appreciable cytoplasm, and had small nuclei. In contrast, the KP model displayed multiple foci of hyperchromatic tumor nodules that were comprised of papillary proliferations of atypical pneumocytes with increased eosinophilic cytoplasm and enlarged nuclei with irregular nuclear contours, nuclear grooves, and vesicular chromatin, consistent with a well-differentiated adenocarcinoma, papillary type. The KP-PI model, of note, exhibited an increased overall tumor burden which nearly completely replaced the lung parenchyma. The tumor cells in this model were forming sheets and clusters with no overt glandular or papillary differentiation. The carcinoma cells showed increased nuclear to cytoplasmic ratios, markedly irregular nuclear contours, variations in nuclear size and shape, and significant nuclear hyperchromasia (Fig. 16H). These findings of KPPI model are consistent with a poorly differentiated adenocarcinoma. Finally, we also tried to test tumor growth rate by immunostaining against Ki67. As shown in Fig. 16I and J, KPPI tumors displayed higher average percentage of Ki67 (19.07%) compared with that of KP tumors (11.30%), indicating KPPI tumors proliferate faster than KP tumors. These data definitely show that PLK1 functions as an oncogene in NSCLC.

5.2.4 PLK1 overexpression results in increased RET expression and enhanced MAPK pathway

RNA sequencing (RNA-seq) analyses were performed to compare KP tumors versus KPPI tumors, and the result showed significantly differential expression of 134 genes, in which 37 were upregulated (Fig. 17A), and 97 were downregulated. Furthermore, Reactome enrichment analysis revealed that upregulated RET, Pbp2 and Psma3 were involved in MAPK pathway activation (Fig. 17B). Besides, we also identified Rhou and EPS8, which regulate Ras protein signal transduction (97, 98), were upregulated upon PLK1 overexpression (Fig. 17A). Among all the genes mentioned above, the gene expression pattern of RET is most similar to that of PLK1 (Fig. 17A), implying it is most likely to be regulated by PLK1. Thus, we decided to select RET as our major study target to decipher the mechanism underlying PLK1's effect on LADC. KPPI tumors displayed an average 2.7-fold change in RET expression compared with KP tumors (Fig. 17C), which was also verified by qRT-PCR (Fig. 17D). To further validate our findings, immunoblots and IHC staining were conducted with KPPI and KP tumors. As shown in Fig 17E and F, RET protein level was higher in KPPI tumors than KP tumors. Notably, p-RET (1086), which is responsible for MAPK pathway and PI3K pathway activation, was also enhanced as RET protein increases (Fig. 17E), resulting in higher levels of p-ERK and p-AKT in KPPI tumors (Fig. 17E).

5.2.5 Elimination of PLK1 results in slower LADC growth and decrease RET expression

Having established that PLK1 elevation promoted progression of LADC and increased RET expression, we tried to validate our findings by knocking out PLK1 in KP model (KPPO). At the 12th week after Ad-cre infection, lung tumors of both KP and KPPO mice were monitored by MRI. Compared with KP mice, KPPO's lungs displayed significantly less tumor burden, with mean value decreased from 54.78% for KP mice to 18.14% for KPPO mice (Fig. 18A and B). Moreover, RET protein levels in tumors were examined by immunoblots and IHC staining. As shown in Fig. 18D and E, less RET was expressed in tumors of KPPO than KP, and the lower level of p-ERK indicates that MAPK pathway activity was reduced as RET decreased (Fig. 18D). Thus, all these data further confirm that PLK1 acts as an oncogene in LADC harboring KP, and promotes MAPK pathway activation, likely via regulating RET.

5.2.6 RET is regulated by PLK1 and necessary for PLK1-overexpressed NSCLC growth

To further study PLK1's role in regulating RET and RET's effect on cell proliferation, we established cell lines from tumors of KP and KPPI mice (mLAC and mLAP, respectively) (Fig. 19A). Consistent with our in vivo data, mLAP displayed higher mRNA level of RET (Fig. 19B), and immunoblots showed increased protein levels of RET and p-ERK caused by PLK1 overexpression (Fig. 19C). Then, we tried to test PLK1's effect on RET by inhibiting it using either shRNA or GSK461 in mLAP. As expected, PLK1 knockdown led to reduced protein level of RET (Fig. 19D), suggesting that RET is regulated by PLK1. Also, RET protein levels gradually decreased as GSK461 concentration increasede (Fig. 19E), indicating that PLK's regulation on RET is kinase-dependent. Next, we asked whether RET was necessary for the growth of PLK1-overexpressed lung tumor cells. As shown in Fig. 19F, mLAP exhibited higher growth rate than mLAC. Notably, RET's ligand GDNF (glial cell line-derived neurotrophic factor) accelerated growth of both cell lines, but with a larger extent in mLAP (Fig. 19F), indicating more RET expression renders cells more sensitive to its ligand. Furthermore, we also observed GDNF strongly increased p-RET and p-ERK in mLAP, but its stimulating effect on RET in mLAC was much weaker (Fig. 19G). To further confirm RET's role, shRNA was used to remove partial RET from mLAP (Fig. 19H). After RET being knocked down, mLAP cells grew more slowly both in vitro and in vivo (Fig. 19I and J). After one-month growth, mLAP-derived tumors with RET knockdown displayed smaller sizes and lighter weights (Fig. 19K and L). Taken together, all these data demonstrate that PLK1 promotes LADC development via regulating RET.

5.3   Discussion

PLK1 has well documented roles in many mitotic related events, such as centrosome maturation, bipolar spindle formation, sister chromatid segregation and cytokinesis (40). Overexpression of PLK1 has been found in various human malignancies (99-105), and it is generally believed that PLK1 elevation is oncogenic. High PLK1 protein level was found to be correlated to poor tumor differentiation, advanced clinical stages and low survival rate in NSCLC patients (41), which is consistent with our bioinformatics analysis (Fig. 1A-C). In order to study PLK1's function in NSCLC, we knocked PLK1 into KP mice model. Compared with KP mice, KPPI displayed lower survival rate, as well as larger tumors with poorer differentiation and higher proliferation rate, which recapitulates the characteristics of human NSCLC progression driven by enhanced PLK1. In addition, we also knocked out PLK1 form KP mice. After elimination of PLK1, it was difficult for KP mice to develop tumors in their lungs, with only a few small tumors found. All together, these data indicate that PLK1 functions as an oncogene during NSCLC development.

Although PLK1 is well-known for its role in cell cycle regulation, increasing evidence suggests that PLK1 might have many functions beyond mitosis (106). Some studies showed that PLK1 positively regulated MAPK pathway (107-109), but the mechanisms underlying it still remains not entirely clear. In our study, one major pathway we identified affected by PLK1 is RET signaling. Overexpression of PLK1 upregulates RET gene expression, while knockout of PLK1 downregulates it. The RET proto-oncogene encodes a receptor tyrosine kinase, whose activation upon binding to its ligand GDNF leads to subsequent activation of MAPK pathway(110). It is well known that Kras and p53 mutations are the most frequent mutations in NSCLC patients, and NSCLC cell lines with Kras^{G12D} mutation preferably activate MAPK and PI3K signaling (111). In our study, the upregulation of RET induced by PLK1 cooperates with Kras^{G12D} to further activate MAPK pathway, promoting lung tumor development. Therefore, combining inhibitors targeting PLK1 or RET with traditional medication of inhibiting MAPL may help the treatment of NSCLC.
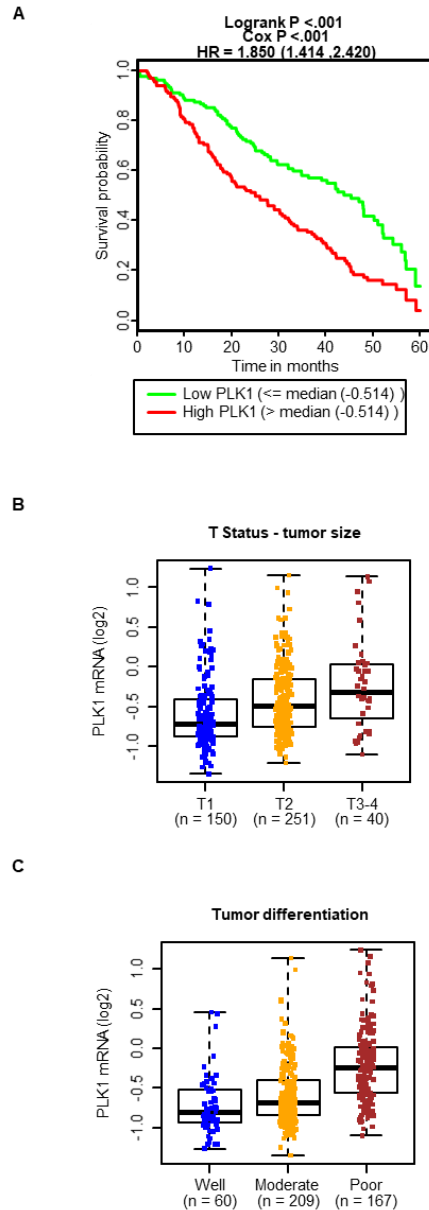
Figure 14. Overexpression of PLK1 correlates with low survival rate of LADC patients, increased tumor size, and poor differentiation.

(A) PLK1 mRNA expression versus the survival rate of LADC patients. The data used in this study was obtained from Oncomine, and it is from Director's Challenge Consortium for the Molecular Classification of LADC. The median split was used to dichotomize the continuous expression levels of PLK1. (B) PLK1 mRNA was higher in T3-4 tumors compared with that in T1 or T2 tumors. (C) PLK1 mRNA was higher in poorly-differentiated tumors compared with that in well-differentiated or moderate-differentiated tumors.
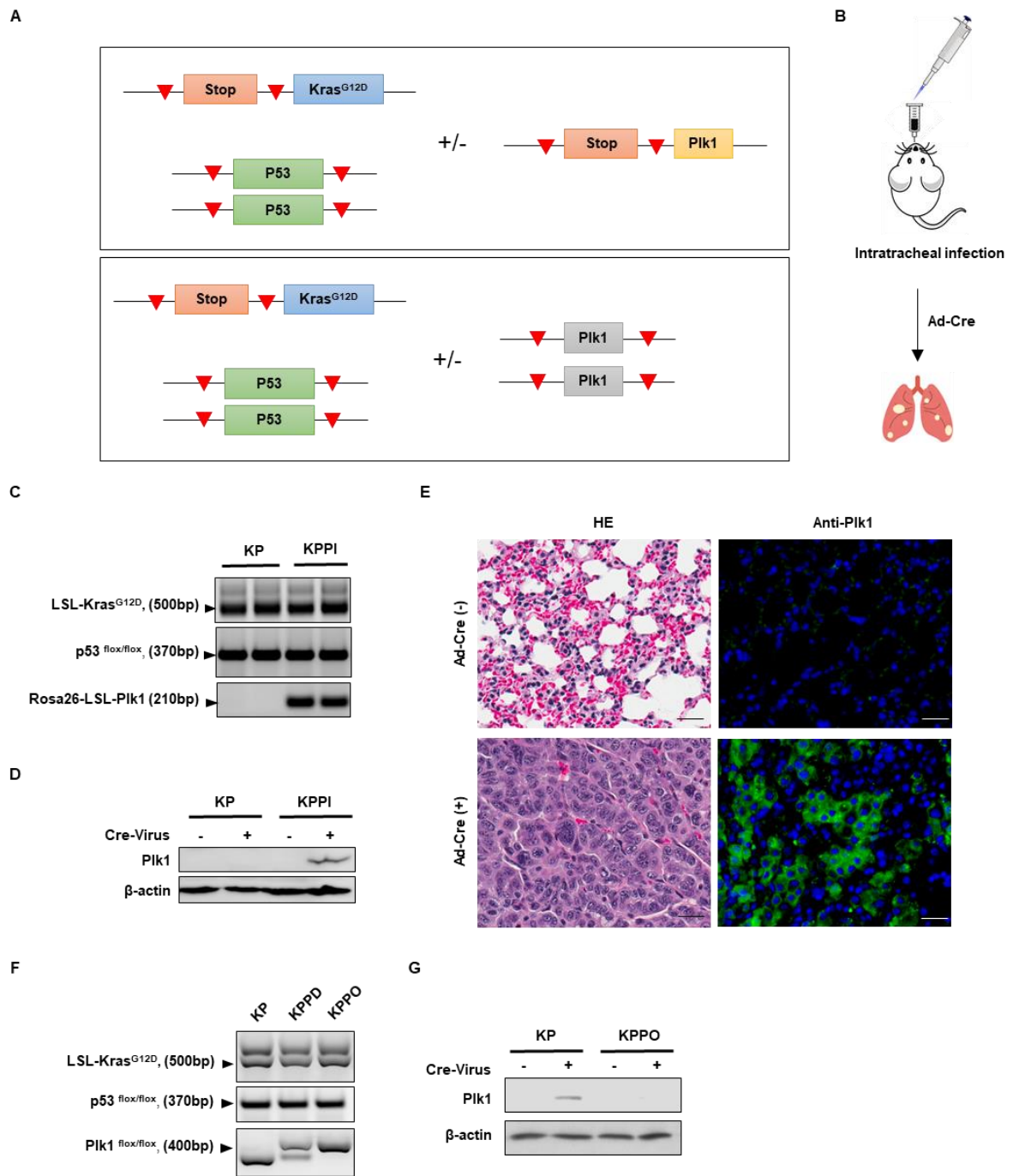
Figure 15. Modification of PLK1 in KP mouse model.

(A) Schematic showing the mice crossing strategy: KP mice were crossed with PLK1 knock-in mice or PLK1 knock-out mice respectively. (B) Schematic showing the intratracheal inhalation of adenovirus-expressing Cre (Ad-Cre), which induces activation of the transgenes. (C) 50 ng of

mouse genomic DNA was analyzed in each PCR to identify banding patterns of indicated transgenes. (D) Immunoblotting results showing amounts of PLK1 in KP and KPPI mice. Tumors are harvested 12 weeks after Ad-Cre infection. (E) Representative H&E stained sections showing tumor formation in KPPI mice after Ad-Cre infection, and immunofluorescence staining against PLK1 of KPPI tumors. The KPPI mouse without Ad-Cre was used as control. Scale bars, 50 μm. (F) 50 ng of mouse genomic DNA was analyzed in each PCR to identify banding patterns of indicated transgenes. (G) Immunoblotting results showing amounts of PLK1 in KP and KPPO mice. Tumors are harvested 14 weeks after Ad-Cre infection.
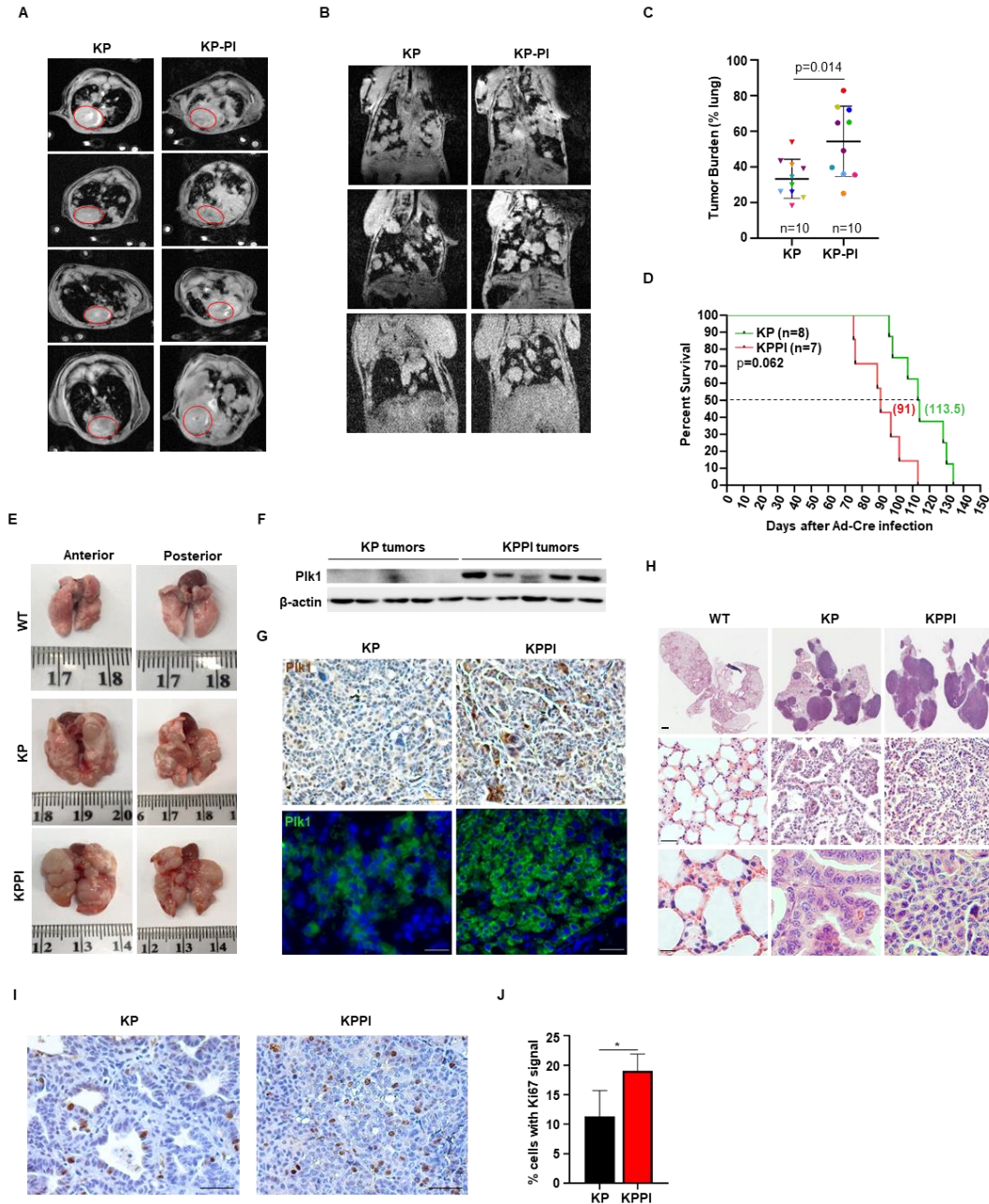
Figure 16. PLK1 overexpression accelerates development of LADC.

(A and B) Representative MRI images of the thorax regions of mice 10 weeks after infection with Ad-Cre. (C) Quantification of MRI. (D) The survival rate of KPPI mice versus KP mice. (E) Representative photographs of lungs 12 weeks after Ad-Cre infection. (F) Representative immunoblotting results of PLK1 protein levels in 5 tumors of either cohort (KP vs. KPPI). (G) Representative IHC staining and immunofluorescence staining for PLK1. Scale bars are 250 μm

and 50 μm respectively. (H) Representative H&E-stained section of tumors. (KP vs. KPPI). Scale bars are 1mm, 250 μm and 100 μm respectively. (I) Representative IHC staining of phospho histone H3 (Ser 10) in primary tumors of mice. Scale bars: 250 μm. (J) Data is presented as ration of positively stained cells to total cells. The p value was calculated using unpaired student t test.
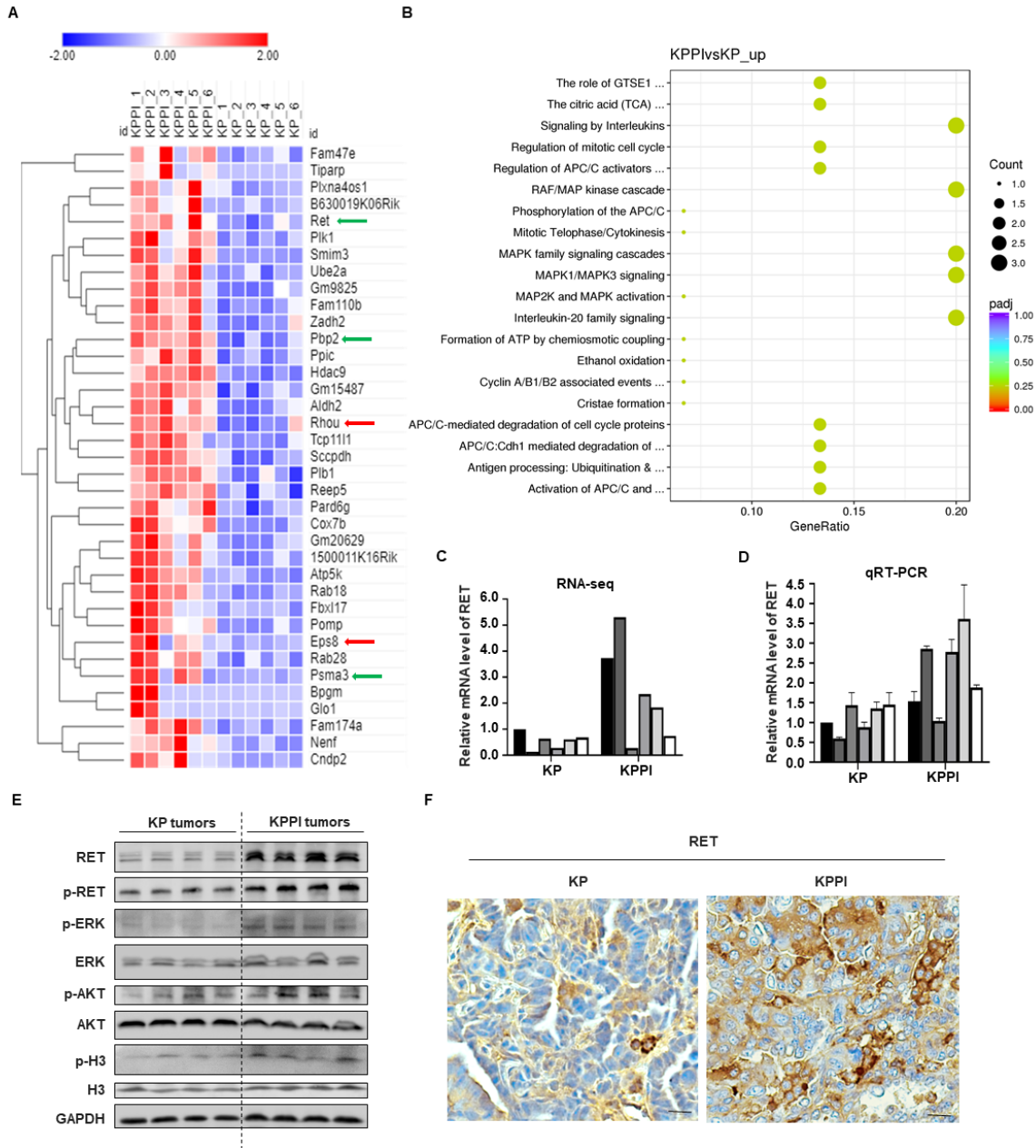
Figure 17. RET expression is enhanced by PLK1.

(A) Heat map of the 37 upregulated genes with PLK1 overexpression in primary tumors. The clustering method is based on the similarity of the gene expression. Blue denotes low expression and red denotes high expression. Green (RNAseq) and red (publication) arrows indicate genes involved in MAPK pathway activation. (B) Histogram of reactome enrichment analysis (KPPI versus KP). Count: the number of differentially expressed genes related to the pathway. Padj: adjusted p-value. (C and D) RNAseq FPKM (fragments per kilobase of transcript sequence per

millions base pairs sequenced) values and qRT-PCR validation of RET in tumors. (E) Western blots on single primary tumor lysates. 4 mice in either cohort were selected. (F) Representative images of IHC staining for RET in KP and KPPI tumors. Scale bars: 100 μm.
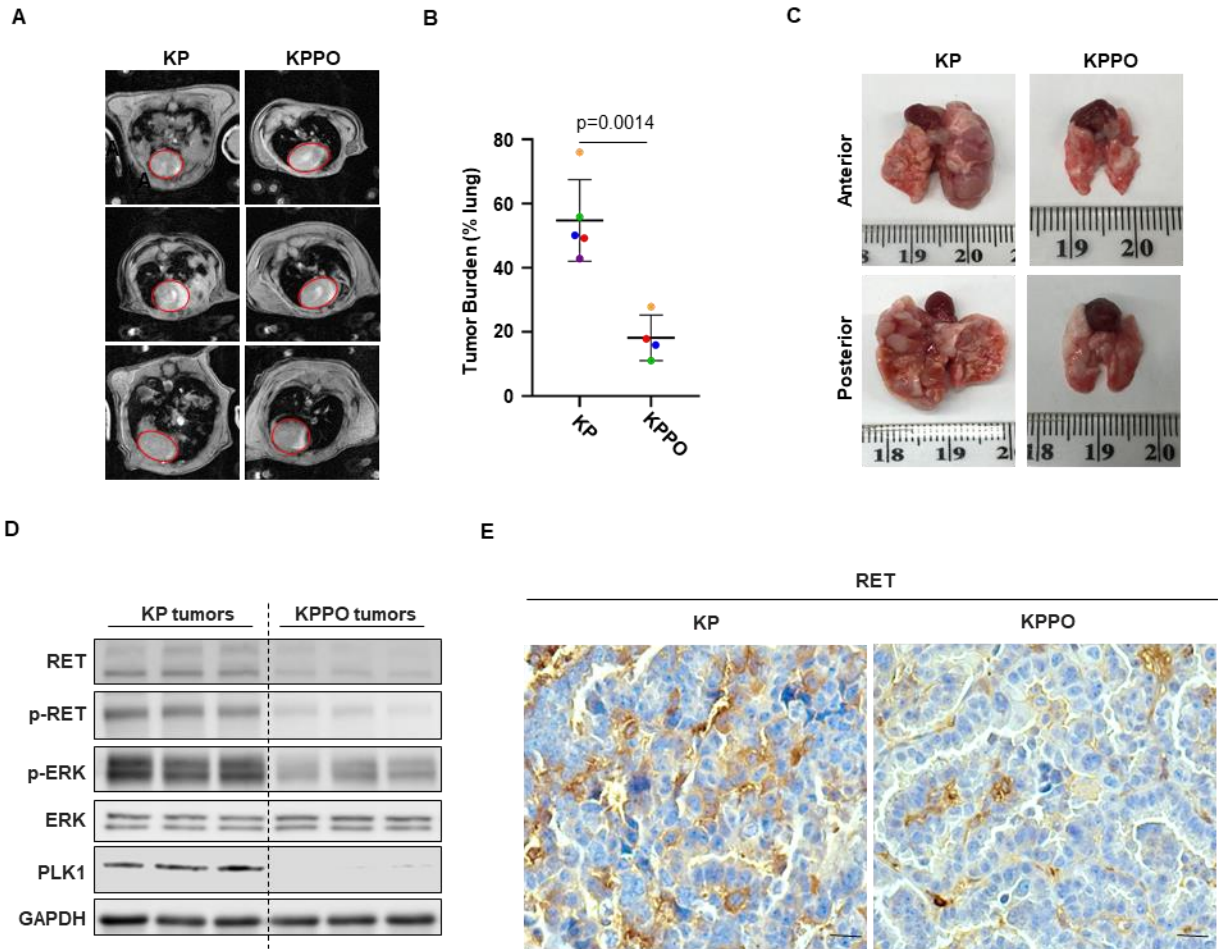
Figure 18. Elimination of PLK1 results in slower LADC growth and decreased RET expression.

(A) Representative MRI images of the thorax regions of mice 12 weeks after infection with Ad-Cre. (B) Quantification of MRI. (C) Representative photographs of lungs 14 weeks after Ad-Cre infection. (D) Western blots on single primary tumor lysates. 3 mice in either cohort were selected. (E) Representative images of IHC staining for RET in KP and KPPO tumors. Scale bars: 100 μm.
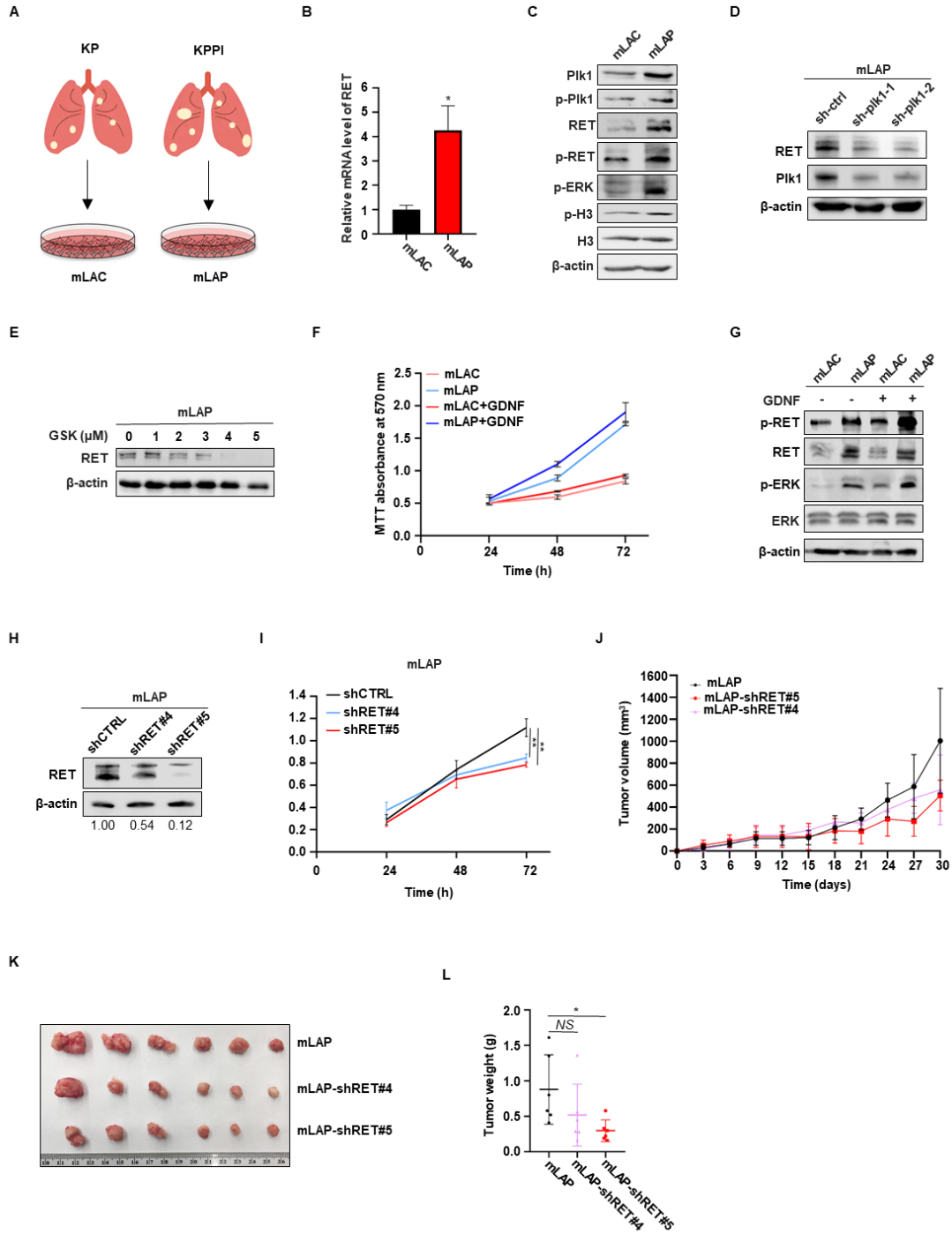
Figure 19. PLK1 promotes LUAC cell growth iva upregulating RET.

Ensure all information remains on the same page as the figure.

(A) Schematic showing that LADC cells were established from KP and KPPI mice 12 weeks after Ad-Cre infection. (B) qRT-PCR analyses of RET mRNA from mLAC and mLAP cells (n=3). Values were normalized to β-actin expression and then to mLAC. (C) Western blots showing

amounts of indicated proteins in mLAC and mLAP cells. (D) Western blots showing decreased amount of RET after PLK1 was knocked down in mLAP cells. (E) mLAP was treated with GSK461364 at the indicated concentrations. After 48 hours, cell lysates were harvested for immunoblotting. (F) Cell viability assay of untreated and GDNF-treated mLAC and mLAP cells. GDNF, 20ng/ml. (G) mLAC and mLAP were treated with vehicle or GDNF (20ng/ml) for 24 hours. Then cell lysates were collected for western blot. (H) Validation by immunoblotting showing knockdown of RET in mLAP cells. (I) Cell viability assay of shRNA-mediated RET knockdown in mLAP cells. (J) 2×10^6 mLAP cells transfected with control shRNA or RET shRNA were subcutaneously incubated into mice. The tumor volumes were measured every 3 days (measn ± S.D.; n=6 for each group) for 30 days. (K) Visualization of fresh tumors harvested from the three groups. (L) The final weights of the harvested xenograft tumors.

CHAPTER 6.   SUMMARY AND FUTURE DIRECTION

6.1   Improvement of treatment for PCa

Since Hodges and Huggins observed that CRPC patients benefited from castration, blocking the function of AR has remained the treatment-objective in clinical therapeutics of the disease. In the future, the existing antiandrogens, used both alone and combined with other treatments, have great potential to strongly promote patients' outcomes in the future. In my study, I found the combination of HMGCR inhibition and enzalutamide inhibited PCa cell growth significantly, and inhibiting HMGCR led to AR degradation. However, the deeper mechanism still remains elusive. It has been shown that PTEN inactivation enhanced AR phosphorylation, promoting p300's acetylation on AR, therefore preventing its ubiquitination and degradation (112). Moreover, AKT has also been demonstrated to promote p300's activity through phosphorylation (113). Thus, it is likely that AR's degradation is mediated by PI3K pathway. Furthermore, Cholesterol is one of the important molecules of lipid rafts which regulate signal transduction, including PI3K pathway and MAPK pathway (14). Therefore, inhibiting HMGCR may downregulate the activity of PI3K pathway, reducing p300's acetylation and increasing AR's degradation. However, more experiments are needed to test this.

Recently, accumulating evidence has shown that EZH2 plays an important role in tumor oncogenesis and progression (28). Also, targeting EZH2 has been shown to be effective to treat prostate cancer (114, 115). Here, I found that AR antagonized EZH2's degradation upon metformin treatment, and this further confirms AR's therapeutic objective in clinical therapy for PCa. Given that metformin can inhibit AR (86), it is also intriguing to test whether the combination between AR antagonists and EZH2's inhibitors is efficient to treat PCa in the future.

6.2   PLK1's role in lung carcinoma

Although PLK1 is well-known for its role in cell cycle regulation, increasing evidence suggests that PLK1 might have many functions beyond mitosis (106). Some studies showed that PLK1 positively regulated MAPK pathway (107-109), and we also identified that PLK1 promoted

MAPK pathway through upregulating RET. However, it still remains elusive that how PLK1 regulates RET expression, and what RET overexpression induces besides activation of MAPK pathway.

The whole process of RET transcription is complicated, in which dynamic interaction occurs among transcription factors and major promoters, and the aberrant RET expression can be resulted from any alternation in this mechanism. The transcription factors, including NKX2.1 (also known as TTF-1), PHOX2B, SOX10, and PAX3, are reported to regulate RET transcription (116). Therefore, it is interesting to investigate whether they are mediators in PLK1's regulation on RET. Given that RET's upregulation induced by PLK1 is kinase dependent, the kinase assay can be conducted in the future to test whether these transcription factors are substrates of PLK1.

Activation of RET, which is glial cell-line derived neurotrophic family ligands (GFL) dependent, occurs in both lung cancer and thyroid cancer via point mutations or rearrangement. However, increasing amount of evidence found that the wild-type RET activation mediated by GFL promoted tumor growth (117), which is consistent with our finding. It has been reported that GFL promoted the development of various neurons, and RET played a vital role in regulating the differentiation and survival of neurons via binding of GDNF (118). Given that neuroendocrine tumors contain comparable properties to neurons (119), it is likely that GFL-RET receptor system regulates the transformation to neuroendocrine carcinoma and the development of neuroendocrine tumors in lung cancer. To study this, morphologic analyses, or molecular analyses targeting CD56, SYN, and CgA can be used. Also, GFL-RET receptor system can considered to be an important molecular target for novel therapeutic methods for NSCLC patients in future.

REFERENCES

1.   Lorente D, Mateo J, Zafeiriou Z, Smith AD, Sandhu S, Ferraldeschi R, et al. Switching and withdrawing hormonal agents for castration-resistant prostate cancer. Nat Rev Urol. 2015;12(1):37-47.
2.   Nyquist MD, Dehm SM. Interplay between genomic alterations and androgen receptor signaling during prostate cancer development and progression. Horm Cancer. 2013;4(2):61-9.
3.   Shiota M, Song Y, Takeuchi A, Yokomizo A, Kashiwagi E, Kuroiwa K, et al. Antioxidant therapy alleviates oxidative stress by androgen deprivation and prevents conversion from androgen dependent to castration resistant prostate cancer. J Urol. 2012;187(2):707-14.
4.   Wang Q, Li W, Zhang Y, Yuan X, Xu K, Yu J, et al. Androgen receptor regulates a distinct transcription program in androgen-independent prostate cancer. Cell. 2009;138(2):245-56.
5.   Attard G, Cooper CS, de Bono JS. Steroid hormone receptors in prostate cancer: a hard habit to break? Cancer Cell. 2009;16(6):458-62.
6.   Claessens F, Helsen C, Prekovic S, Van den Broeck T, Spans L, Van Poppel H, et al. Emerging mechanisms of enzalutamide resistance in prostate cancer. Nat Rev Urol. 2014;11(12):712-6.
7.   Marques RB, Dits NF, Erkens-Schulze S, van Weerden WM, Jenster G. Bypass mechanisms of the androgen receptor pathway in therapy-resistant prostate cancer cell models. PLoS One. 2010;5(10):e13500.
8.   Haag P, Bektic J, Bartsch G, Klocker H, Eder IE. Androgen receptor down regulation by small interference RNA induces cell growth inhibition in androgen sensitive as well as in androgen independent prostate cancer cells. J Steroid Biochem Mol Biol. 2005;96(3-4):251-8.
9.   Denmeade SR, Lin XS, Isaacs JT. Role of programmed (apoptotic) cell death during the progression and therapy for prostate cancer. Prostate. 1996;28(4):251-65.
10.   Tu JJ, Rohan S, Kao J, Kitabayashi N, Mathew S, Chen YT. Gene fusions between TMPRSS2 and ETS family genes in prostate cancer: frequency and transcript variant analysis by RT-PCR and FISH on paraffin-embedded tissues. Mod Pathol. 2007;20(9):921-8.
11.   Arora VK, Schenkein E, Murali R, Subudhi SK, Wongvipat J, Balbas MD, et al. Glucocorticoid receptor confers resistance to antiandrogens by bypassing androgen receptor blockade. Cell. 2013;155(6):1309-22.
12.   Gao H, Ouyang X, Banach-Petrosky WA, Shen MM, Abate-Shen C. Emergence of androgen independence at early stages of prostate cancer progression in Nkx3.1; Pten mice. Cancer Res. 2006;66(16):7929-33.
13.   Mullen PJ, Yu R, Longo J, Archer MC, Penn LZ. The interplay between cell signalling and the mevalonate pathway in cancer. Nat Rev Cancer. 2016;16(11):718-31.
14.   Mollinedo F, Gajate C. Lipid rafts as major platforms for signaling regulation in cancer. Adv Biol Regul. 2015;57:130-46.
15.   Ko YJ, Balk SP. Targeting steroid hormone receptor pathways in the treatment of hormone dependent cancers. Curr Pharm Biotechnol. 2004;5(5):459-70.
16.   Sharpe LJ, Brown AJ. Controlling cholesterol synthesis beyond 3-hydroxy-3-methylglutaryl-CoA reductase (HMGCR). J Biol Chem. 2013;288(26):18707-15.
17.   Vivanco I, Sawyers CL. The phosphatidylinositol 3-Kinase AKT pathway in human cancer. Nat Rev Cancer. 2002;2(7):489-501.
18.   Bitting RL, Armstrong AJ. Targeting the PI3K/Akt/mTOR pathway in castration-resistant prostate cancer. Endocr Relat Cancer. 2013;20(3):R83-99.

19.   Di Cristofano A, Pesce B, Cordon-Cardo C, Pandolfi PP. Pten is essential for embryonic development and tumour suppression. Nat Genet. 1998;19(4):348-55.
20.   Ni J, Liu Q, Xie S, Carlson C, Von T, Vogel K, et al. Functional characterization of an isoform-selective inhibitor of PI3K-p110beta as a potential anticancer agent. Cancer Discov. 2012;2(5):425-33.
21.   Schwartz S, Wongvipat J, Trigwell CB, Hancox U, Carver BS, Rodrik-Outmezguine V, et al. Feedback suppression of PI3Kalpha signaling in PTEN-mutated tumors is relieved by selective inhibition of PI3Kbeta. Cancer Cell. 2015;27(1):109-22.
22.   Kasznicki J, Sliwinska A, Drzewoski J. Metformin in cancer prevention and therapy. Ann Transl Med. 2014;2(6):57.
23.   Spratt DE, Zhang C, Zumsteg ZS, Pei X, Zhang Z, Zelefsky MJ. Metformin and prostate cancer: reduced development of castration-resistant disease and prostate cancer mortality. Eur Urol. 2013;63(4):709-16.
24.   Murtola TJ, Tammela TL, Lahtela J, Auvinen A. Antidiabetic medication and prostate cancer risk: a population-based case-control study. Am J Epidemiol. 2008;168(8):925-31.
25.   Rothermundt C, Hayoz S, Templeton AJ, Winterhalder R, Strebel RT, Bartschi D, et al. Metformin in chemotherapy-naive castration-resistant prostate cancer: a multicenter phase 2 trial (SAKK 08/09). Eur Urol. 2014;66(3):468-74.
26.   Li K, Si-Tu J, Qiu J, Lu L, Mao Y, Zeng H, et al. Statin and metformin therapy in prostate cancer patients with hyperlipidemia who underwent radiotherapy: a population-based cohort study. Cancer Manag Res. 2019;11:1189-97.
27.   Simon JA, Kingston RE. Mechanisms of polycomb gene silencing: knowns and unknowns. Nat Rev Mol Cell Biol. 2009;10(10):697-708.
28.   Shen L, Cui J, Liang S, Pang Y, Liu P. Update of research on the role of EZH2 in cancer progression. Onco Targets Ther. 2013;6:321-4.
29.   Yap TA, Winter JN, Leonard JP, Ribrag V, Constantinidou A, Giulino-Roth L, et al. A Phase I Study of GSK2816126, an Enhancer of Zeste Homolog 2(EZH2) Inhibitor, in Patients (pts) with Relapsed/Refractory Diffuse Large B-Cell Lymphoma (DLBCL), Other Non-Hodgkin Lymphomas (NHL), Transformed Follicular Lymphoma (tFL), Solid Tumors and Multiple Myeloma (MM). 2016;128(22):4203-.
30.   Gonzalez ME, DuPrie ML, Krueger H, Merajver SD, Ventura AC, Toy KA, et al. Histone methyltransferase EZH2 induces Akt-dependent genomic instability and BRCA1 inhibition in breast cancer. Cancer Res. 2011;71(6):2360-70.
31.   Kim J, Lee Y, Lu X, Song B, Fong KW, Cao Q, et al. Polycomb- and Methylation-Independent Roles of EZH2 as a Transcription Activator. Cell Rep. 2018;25(10):2808-20 e4.
32.   Siegel RL, Miller KD, Jemal A. Cancer statistics, 2019. CA Cancer J Clin. 2019;69(1):7-34.
33.   Shames DS, Wistuba, II. The evolving genomic classification of lung cancer. J Pathol. 2014;232(2):121-33.
34.   Seki A, Coppinger JA, Jang CY, Yates JR, Fang G. Bora and the kinase Aurora a cooperatively activate the kinase Plk1 and control mitotic entry. Science. 2008;320(5883):1655-8.
35.   Golsteyn RM, Mundt KE, Fry AM, Nigg EA. Cell cycle regulation of the activity and subcellular localization of Plk1, a human protein kinase implicated in mitotic spindle function. J Cell Biol. 1995;129(6):1617-28.
36.   Elowe S, Hummer S, Uldschmid A, Li X, Nigg EA. Tension-sensitive Plk1 phosphorylation on BubR1 regulates the stability of kinetochore microtubule interactions. Genes Dev. 2007;21(17):2205-19.

37. Lane HA, Nigg EA. Antibody microinjection reveals an essential role for human polo-like kinase 1 (Plk1) in the functional maturation of mitotic centrosomes. J Cell Biol. 1996;135(6 Pt 2):1701-13.

38. Neef R, Preisinger C, Sutcliffe J, Kopajtich R, Nigg EA, Mayer TU, et al. Phosphorylation of mitotic kinesin-like protein 2 by polo-like kinase 1 is required for cytokinesis. J Cell Biol. 2003;162(5):863-75.

39. Schmidt A, Duncan PI, Rauh NR, Sauer G, Fry AM, Nigg EA, et al. Xenopus polo-like kinase Plx1 regulates XErp1, a novel inhibitor of APC/C activity. Genes Dev. 2005;19(4):502-13.

40. Strebhardt K. Multifaceted polo-like kinases: drug targets and antitargets for cancer therapy. Nat Rev Drug Discov. 2010;9(8):643-60.

41. Wang ZX, Xue D, Liu ZL, Lu BB, Bian HB, Pan X, et al. Overexpression of polo-like kinase 1 and its clinical significance in human non-small cell lung cancer. Int J Biochem Cell Biol. 2012;44(1):200-10.

42. Li H, Wang H, Sun Z, Guo Q, Shi H, Jia Y. The clinical and prognostic value of polo-like kinase 1 in lung squamous cell carcinoma patients: immunohistochemical analysis. Biosci Rep. 2017;37(4).

43. Stratmann JA, Sebastian M. Polo-like kinase 1 inhibition in NSCLC: mechanism of action and emerging predictive biomarkers. Lung Cancer (Auckl). 2019;10:67-80.

44. Peng Q, Deng Z, Pan H, Gu L, Liu O, Tang Z. Mitogen-activated protein kinase signaling pathway in oral cancer. Oncol Lett. 2018;15(2):1379-88.

45. Hommes DW, Peppelenbosch MP, van Deventer SJ. Mitogen activated protein (MAP) kinase signal transduction pathways and novel anti-inflammatory targets. Gut. 2003;52(1):144-51.

46. Fang JY, Richardson BC. The MAPK signalling pathways and colorectal cancer. Lancet Oncol. 2005;6(5):322-7.

47. Pradhan R, Singhvi G, Dubey SK, Gupta G, Dua K. MAPK pathway: a potential target for the treatment of non-small-cell lung carcinoma. Future Med Chem. 2019;11(8):793-5.

48. Sakurai M, Hayashi T, Abe K, Itoyuama Y, Tabayashi K. Induction of phosphatidylinositol 3-kinase and serine-threonine kinase-like immunoreactivity in rabbit spinal cord after transient ischemia. Neurosci Lett. 2001;302(1):17-20.

49. Plaza-Menacho I, Mologni L, McDonald NQ. Mechanisms of RET signaling in cancer: current and future implications for targeted therapy. Cell Signal. 2014;26(8):1743-52.

50. Besset V, Scott RP, Ibanez CF. Signaling complexes and protein-protein interactions involved in the activation of the Ras and phosphatidylinositol 3-kinase pathways by the c-Ret receptor tyrosine kinase. J Biol Chem. 2000;275(50):39159-66.

51. Hayashi H, Ichihara M, Iwashita T, Murakami H, Shimono Y, Kawai K, et al. Characterization of intracellular signals via tyrosine 1062 in RET activated by glial cell line-derived neurotrophic factor. Oncogene. 2000;19(39):4469-75.

52. Segouffin-Cariou C, Billaud M. Transforming ability of MEN2A-RET requires activation of the phosphatidylinositol 3-kinase/AKT signaling pathway. J Biol Chem. 2000;275(5):3568-76.

53. Sunaga N, Kaira K, Imai H, Shimizu K, Nakano T, Shames DS, et al. Oncogenic KRAS-induced epiregulin overexpression contributes to aggressive phenotype and is a promising therapeutic target in non-small-cell lung cancer. Oncogene. 2013;32(34):4034-42.

54. Ju YS, Lee WC, Shin JY, Lee S, Bleazard T, Won JK, et al. A transforming KIF5B and RET gene fusion in lung adenocarcinoma revealed from whole-genome and transcriptome sequencing. Genome Res. 2012;22(3):436-45.

55. Kohno T, Ichikawa H, Totoki Y, Yasuda K, Hiramoto M, Nammo T, et al. KIF5B-RET fusions in lung adenocarcinoma. Nat Med. 2012;18(3):375-7.

56. Li Z, Liu J, Li J, Kong Y, Sandusky G, Rao X, et al. Polo-like kinase 1 (Plk1) overexpression enhances ionizing radiation-induced cancer formation in mice. J Biol Chem. 2017;292(42):17461-72.

57. Wachowicz P, Fernandez-Miranda G, Marugan C, Escobar B, de Carcer G. Genetic depletion of Polo-like kinase 1 leads to embryonic lethality due to mitotic aberrancies. Bioessays. 2016;38 Suppl 1:S96-S106.

58. DuPage M, Dooley AL, Jacks T. Conditional mouse lung cancer models using adenoviral or lentiviral delivery of Cre recombinase. Nat Protoc. 2009;4(7):1064-72.

59. Rodriguez-Vida A, Galazi M, Rudman S, Chowdhury S, Sternberg CN. Enzalutamide for the treatment of metastatic castration-resistant prostate cancer. Drug Des Devel Ther. 2015;9:3325-39.

60. Hager MH, Solomon KR, Freeman MR. The role of cholesterol in prostate cancer. Curr Opin Clin Nutr Metab Care. 2006;9(4):379-85.

61. Mittal A, Sathian B, Chandrasekharan N, Lekhi A, Yadav SK. Role of hypercholesterolemia in prostate cancer--case control study from Manipal Teaching Hospital Pokhara, Nepal. Asian Pac J Cancer Prev. 2011;12(8):1905-7.

62. Shafique K, McLoone P, Qureshi K, Leung H, Hart C, Morrison DS. Cholesterol and the risk of grade-specific prostate cancer incidence: evidence from two large prospective cohort studies with up to 37 years' follow up. BMC Cancer. 2012;12:25.

63. Zhong S, Zhang X, Chen L, Ma T, Tang J, Zhao J. Statin use and mortality in cancer patients: Systematic review and meta-analysis of observational studies. Cancer Treat Rev. 2015;41(6):554-67.

64. Hamilton RJ, Goldberg KC, Platz EA, Freedland SJ. The influence of statin medications on prostate-specific antigen levels. Journal of the National Cancer Institute. 2008;100(21):1511-8.

65. Akduman B, Tandberg DJ, O'Donnell CI, Hughes A, Moyad MA, Crawford ED. Effect of Statins on Serum Prostate-specific Antigen Levels. Urology. 2010;76(5):1048-51.

66. Yang L, Egger M, Plattner R, Klocker H, Eder IE. Lovastatin causes diminished PSA secretion by inhibiting AR expression and function in LNCaP prostate cancer cells. Urology. 2011;77(6):1508.e1-7.

67. Yokomizo A, Shiota M, Kashiwagi E, Kuroiwa K, Tatsugami K, Inokuchi J, et al. Statins reduce the androgen sensitivity and cell proliferation by decreasing the androgen receptor protein in prostate cancer cells. Prostate. 2011;71(3):298-304.

68. Zhang Z, Hou X, Shao C, Li J, Cheng JX, Kuang S, et al. Plk1 inhibition enhances the efficacy of androgen signaling blockade in castration-resistant prostate cancer. Cancer Res. 2014;74(22):6635-47.

69. Shao C, Li Z, Ahmad N, Liu X. Regulation of PTEN degradation and NEDD4-1 E3 ligase activity by Numb. Cell Cycle. 2017;16(10):957-67.

70. Scher HI, Beer TM, Higano CS, Anand A, Taplin ME, Efstathiou E, et al. Antitumour activity of MDV3100 in castration-resistant prostate cancer: a phase 1-2 study. Lancet (London, England). 2010;375(9724):1437-46.

71. TJ M, H S, P P, M B, T S, T Y, et al. - The importance of LDL and cholesterol metabolism for prostate epithelial cell. - PLoS One 2012;7(6):e39445 doi: 101371/journalpone0039445 Epub 2012 Jun 27. (- 1932-6203 (Electronic)):- e39445.

72. Horgan AM, Seruga B, Pond GR, Alibhai SM, Amir E, De Wit R, et al. Tolerability and efficacy of docetaxel in older men with metastatic castrate-resistant prostate cancer (mCRPC) in the TAX 327 trial. J Geriatr Oncol. 2014;5(2):119-26.

73. Leibowitz-Amit R, Templeton AJ, Alibhai SM, Knox JJ, Sridhar SS, Tannock IF, et al. Efficacy and toxicity of abiraterone and docetaxel in octogenarians with metastatic castration-resistant prostate cancer. J Geriatr Oncol. 2015;6(1):23-8.

74. Stopsack KH, Gerke TA, Andren O, Andersson SO, Giovannucci EL, Mucci LA, et al. Cholesterol uptake and regulation in high-grade and lethal prostate cancers. Carcinogenesis. 2017;38(8):806-11.

75. Han W, Gao S, Barrett D, Ahmed M, Han D, Macoska JA, et al. Reactivation of androgen receptor-regulated lipid biosynthesis drives the progression of castration-resistant prostate cancer. Oncogene. 2018;37(6):710-21.

76. Liu C, Lou W, Zhu Y, Yang JC, Nadiminty N, Gaikwad NW, et al. Intracrine Androgens and AKR1C3 Activation Confer Resistance to Enzalutamide in Prostate Cancer. Cancer Res. 2015;75(7):1413-22.

77. Sekine Y, Furuya Y, Nishii M, Koike H, Matsui H, Suzuki K. Simvastatin inhibits the proliferation of human prostate cancer PC-3 cells via down-regulation of the insulin-like growth factor 1 receptor. Biochem Biophys Res Commun. 2008;372(2):356-61.

78. Hong MY, Seeram NP, Zhang Y, Heber D. Chinese red yeast rice versus lovastatin effects on prostate cancer cells with and without androgen receptor overexpression. Journal of medicinal food. 2008;11(4):657-66.

79. Syvala H, Pennanen P, Blauer M, Tammela TL, Murtola TJ. Additive inhibitory effects of simvastatin and enzalutamide on androgen-sensitive LNCaP and VCaP prostate cancer cells. Biochem Biophys Res Commun. 2016;481(1-2):46-50.

80. McCabe MT, Ott HM, Ganji G, Korenchuk S, Thompson C, Van Aller GS, et al. EZH2 inhibition as a therapeutic strategy for lymphoma with EZH2-activating mutations. Nature. 2012;492(7427):108-12.

81. Ren G, Baritaki S, Marathe H, Feng J, Park S, Beach S, et al. Polycomb protein EZH2 regulates tumor invasion via the transcriptional repression of the metastasis suppressor RKIP in breast and prostate cancer. Cancer Res. 2012;72(12):3091-104.

82. Yang YA, Yu J. EZH2, an epigenetic driver of prostate cancer. Protein Cell. 2013;4(5):331-41.

83. Li W, Yuan Y, Huang L, Qiao M, Zhang Y. Metformin alters the expression profiles of microRNAs in human pancreatic cancer cells. Diabetes Res Clin Pract. 2012;96(2):187-95.

84. Bao B, Wang Z, Ali S, Ahmad A, Azmi AS, Sarkar SH, et al. Metformin inhibits cell proliferation, migration and invasion by attenuating CSC function mediated by deregulating miRNAs in pancreatic cancer cells. Cancer Prev Res (Phila). 2012;5(3):355-64.

85. Yamaguchi H, Hung MC. Regulation and Role of EZH2 in Cancer. Cancer Res Treat. 2014;46(3):209-22.

86. Wang Y, Liu G, Tong D, Parmar H, Hasenmayer D, Yuan W, et al. Metformin represses androgen-dependent and androgen-independent prostate cancers by targeting androgen receptor. Prostate. 2015;75(11):1187-96.

87. Xu K, Wu ZJ, Groner AC, He HH, Cai C, Lis RT, et al. EZH2 oncogenic activity in castration-resistant prostate cancer cells is Polycomb-independent. Science. 2012;338(6113):1465-9.

88. Shao C, Ahmad N, Hodges K, Kuang S, Ratliff T, Liu X. Inhibition of polo-like kinase 1 (Plk1) enhances the antineoplastic activity of metformin in prostate cancer. J Biol Chem. 2015;290(4):2024-33.

89.   Chen L, Ahmad N, Liu X. Combining p53 stabilizers with metformin induces synergistic apoptosis through regulation of energy metabolism in castration-resistant prostate cancer. Cell Cycle. 2016;15(6):840-9.

90.   Bishop JL, Thaper D, Vahid S, Davies A, Ketola K, Kuruma H, et al. The Master Neural Transcription Factor BRN2 Is an Androgen Receptor-Suppressed Driver of Neuroendocrine Differentiation in Prostate Cancer. Cancer Discov. 2017;7(1):54-71.

91.   Pasqualini L, Bu H, Puhr M, Narisu N, Rainer J, Schlick B, et al. miR-22 and miR-29a Are Members of the Androgen Receptor Cistrome Modulating LAMC1 and Mcl-1 in Prostate Cancer. Mol Endocrinol. 2015;29(7):1037-54.

92.   Takayama KI, Misawa A, Inoue S. Significance of microRNAs in Androgen Signaling and Prostate Cancer Progression. Cancers (Basel). 2017;9(8).

93.   Kim E, Kim M, Woo DH, Shin Y, Shin J, Chang N, et al. Phosphorylation of EZH2 activates STAT3 signaling via STAT3 methylation and promotes tumorigenicity of glioblastoma stem-like cells. Cancer Cell. 2013;23(6):839-52.

94.   Graham GG, Punt J, Arora M, Day RO, Doogue MP, Duong JK, et al. Clinical pharmacokinetics of metformin. Clin Pharmacokinet. 2011;50(2):81-98.

95.   Vecchio S, Giampreti A, Petrolini VM, Lonati D, Protti A, Papa P, et al. Metformin accumulation: lactic acidosis and high plasmatic metformin levels in a retrospective case series of 66 patients on chronic therapy. Clin Toxicol (Phila). 2014;52(2):129-35.

96.   Director's Challenge Consortium for the Molecular Classification of Lung A, Shedden K, Taylor JM, Enkemann SA, Tsao MS, Yeatman TJ, et al. Gene expression-based survival prediction in lung adenocarcinoma: a multi-site, blinded validation study. Nat Med. 2008;14(8):822-7.

97.   Maa MC, Hsieh CY, Leu TH. Overexpression of p97Eps8 leads to cellular transformation: implication of pleckstrin homology domain in p97Eps8-mediated ERK activation. Oncogene. 2001;20(1):106-12.

98.   Zhang JS, Koenig A, Young C, Billadeau DD. GRB2 couples RhoU to epidermal growth factor receptor signaling and cell migration. Mol Biol Cell. 2011;22(12):2119-30.

99.   Weichert W, Schmidt M, Gekeler V, Denkert C, Stephan C, Jung K, et al. Polo-like kinase 1 is overexpressed in prostate cancer and linked to higher tumor grades. Prostate. 2004;60(3):240-5.

100.   Schmit TL, Zhong W, Nihal M, Ahmad N. Polo-like kinase 1 (Plk1) in non-melanoma skin cancers. Cell Cycle. 2009;8(17):2697-702.

101.   Feng YB, Lin DC, Shi ZZ, Wang XC, Shen XM, Zhang Y, et al. Overexpression of PLK1 is associated with poor survival by inhibiting apoptosis via enhancement of survivin level in esophageal squamous cell carcinoma. Int J Cancer. 2009;124(3):578-88.

102.   Jang YJ, Kim YS, Kim WH. Oncogenic effect of Polo-like kinase 1 expression in human gastric carcinomas. Int J Oncol. 2006;29(3):589-94.

103.   Kneisel L, Strebhardt K, Bernd A, Wolter M, Binder A, Kaufmann R. Expression of polo-like kinase (PLK1) in thin melanomas: a novel marker of metastatic disease. J Cutan Pathol. 2002;29(6):354-8.

104.   Shi W, Alajez NM, Bastianutto C, Hui AB, Mocanu JD, Ito E, et al. Significance of Plk1 regulation by miR-100 in human nasopharyngeal cancer. Int J Cancer. 2010;126(9):2036-48.

105.   Takahashi T, Sano B, Nagata T, Kato H, Sugiyama Y, Kunieda K, et al. Polo-like kinase 1 (PLK1) is overexpressed in primary colorectal cancers. Cancer Sci. 2003;94(2):148-52.

106.   Liu XS, Song B, Liu X. The substrates of Plk1, beyond the functions in mitosis. Protein Cell. 2010;1(11):999-1010.

107. Dang SC, Fan YY, Cui L, Chen JX, Qu JG, Gu M. PLK1 as a potential prognostic marker of gastric cancer through MEK-ERK pathway on PDTX models. Onco Targets Ther. 2018;11:6239-47.
108. Jiang S, Tang DD. Plk1 regulates MEK1/2 and proliferation in airway smooth muscle cells. Respir Res. 2015;16:93.
109. Wu J, Ivanov AI, Fisher PB, Fu Z. Polo-like kinase 1 induces epithelial-to-mesenchymal transition and promotes epithelial cell motility by activating CRAF/ERK signaling. Elife. 2016;5.
110. Gainor JF, Shaw AT. The new kid on the block: RET in lung cancer. Cancer Discov. 2013;3(6):604-6.
111. Ricciuti B, Leonardi GC, Metro G, Grignani F, Paglialunga L, Bellezza G, et al. Targeting the KRAS variant for treatment of non-small cell lung cancer: potential therapeutic applications. Expert Rev Respir Med. 2016;10(1):53-68.
112. Zhong J, Ding L, Bohrer LR, Pan Y, Liu P, Zhang J, et al. p300 acetyltransferase regulates androgen receptor degradation and PTEN-deficient prostate tumorigenesis. Cancer Res. 2014;74(6):1870-80.
113. Huang WC, Chen CC. Akt phosphorylation of p300 at Ser-1834 is essential for its histone acetyltransferase and transcriptional activity. Mol Cell Biol. 2005;25(15):6592-602.
114. Han Li C, Chen Y. Targeting EZH2 for cancer therapy: progress and perspective. Curr Protein Pept Sci. 2015;16(6):559-70.
115. Yamagishi M, Uchimaru K. Targeting EZH2 in cancer therapy. Curr Opin Oncol. 2017;29(5):375-81.
116. Leon TY, Ngan ES, Poon HC, So MT, Lui VC, Tam PK, et al. Transcriptional regulation of RET by Nkx2-1, Phox2b, Sox10, and Pax3. J Pediatr Surg. 2009;44(10):1904-12.
117. Mulligan LM. GDNF and the RET Receptor in Cancer: New Insights and Therapeutic Potential. Front Physiol. 2018;9:1873.
118. Ichihara M, Murakumo Y, Takahashi M. RET and neuroendocrine tumors. Cancer Lett. 2004;204(2):197-211.
119. Rudin CM, Drilon A, Poirier JT. RET mutations in neuroendocrine tumors: including small-cell lung cancer. J Thorac Oncol. 2014;9(9):1240-2.